A Blind Spot in the LVRT Current Requirements of Modern Grid Codes for Inverter-Based Resources

Ali Azizi, Amin Banaiemoqadam, Ali Hooshyar, *Senior Member, IEEE*, and Manish Patel, *Senior Member, IEEE*

***Abstract*—Modern grid codes (GCs) require that inverter-based resources (IBRs) inject both positive- and negative-sequence currents during asymmetrical low-voltage ride through (LVRT) conditions. This GC provision prioritizes the reactive currents and also demands maximizing the active positive-sequence current if the IBR has unused current generation capacity when the required reactive current is generated. A variety of inverter control schemes are available to generate positive- and negative-sequence active/reactive currents, and satisfying these GCs seems to be straightforward. However, this paper reveals that the reference current generation methods of existing inverter control schemes fail to fulfil some important requirements of recent GCs. For example, they do not fully utilize the inverter capacity to generate the maximum active and/or reactive current. It is shown that these so-far hidden GC violations can result in a large untapped generation capacity during asymmetrical faults. This paper also develops an algorithm that satisfies recent GCs by deriving the positive- and negative-sequence currents that maximize the IBR's reactive and active currents while the reactive current is prioritized. The simulation of a grid with high IBR penetration verifies that this new algorithm can unlock the full potential of recent GCs by significantly increasing the power generated during LVRT.**

***Index Terms*—Fault current, grid codes (GCs), inverter-based resources (IBRs), low-voltage ride-through (LVRT).**

I. Introduction

THE GRID codes (GCs) usually standardize the operation of inverter-based resources (IBRs) during low-voltage ride-through (LVRT) conditions. Conventional GCs required that the IBRs support the voltage during LVRT by injecting positive-sequence reactive current [1], [2]. More recently, however, some GCs mandate the generation of negative-sequence reactive current as well [3], [4]. As shown in Fig. 1, these GCs require that an IBR's superimposed positive- and negative-sequence reactive currents during LVRT be proportional to their respective voltage changes. In this figure, Δ, Q, $+$, and $-$ denote the superimposed, reactive, positive-sequence, and negative-sequence components, respectively. The curve's slope, K, is usually between 2 to 6.

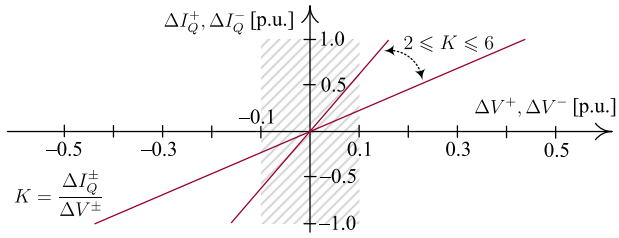

Fig. 1. LVRT current requirement of [3], [4] for IBRs (Negative I_Q is capacitive).

Regardless of the GC, an inverter's phase currents must be limited [5], necessitating a prioritization scheme for different components of current. Recent GCs typically give higher priority to the reactive component of an IBR's LVRT current over its active component. Once the reactive current requirement in Fig. 1 is satisfied, the inverter's remaining capacity must be used to maximize the magnitude of the positive-sequence active current, $|I_P^+|$ [3], [4]. Maximizing the IBR's active current (after prioritizing the reactive currents) is mandated, for example, in Sub-clauses 10.2.3.3 and 4.7.4.2.1.1 of [3] and [4], respectively. Meanwhile, depending on $\Delta V^\pm$, the $\Delta I_Q^\pm$ given by Fig. 1 may lead to phase currents beyond the inverter's limit. Under such conditions, ΔI_Q^+ and ΔI_Q^- are scaled down, preferably uniformly, to limit the phase current [3], [4]. The scaling factor for $\Delta I_Q^\pm$ must be maximized to ensure minimum deviation from the original $\Delta I_Q^\pm$ given by Fig. 1. Thus, this LVRT requirement can be summarized as prioritization/maximization of $\Delta I_Q^\pm$ and maximization of $|I_P^+|$ while the phase current limit of an inverter is met.

The literature on generation of the negative-sequence current for inverters during LVRT does not satisfy the above requirements. For example, the currents derived in [6]–[11] do not ensure full utilization of the IBR's phase current capacity under all LVRT conditions to maximize the magnitudes of the reactive currents,$|I_Q^\pm|$, and $|I_P^+|$. In addition, ΔI_Q^+ and ΔI_Q^- are not necessarily prioritized over $|I_P^+|$ in [8]–[11]. Furthermore, the schemes in [7], [8], [10], [12]–[14] violate the GCs by generating active negative-sequence current, I_P^-.

Within the industrial community, the conventional wisdom holds that recent GCs offer all of the details needed to determine the reference currents: the inverter attempts to meet

Manuscript received 1 December 2021; revised 12 March 2022 and 19 May 2022; accepted 23 June 2022. Date of publication 29 June 2022; date of current version 24 January 2023. Paper no. TPWRD-01756-2021. *(Corresponding authors: Ali Azizi; Ali Hooshyar.)*

Ali Azizi and Ali Hooshyar are with the Department of Electrical and Computer Engineering, University of Toronto, Toronto, ON M5S 3G4, Canada (e-mail: ali.azizi@mail.utoronto.ca; hooshyar@ece.utoronto.ca).

Amin Banaiemoqadam is with the GE Renewable Energy, Markham, ON L6C 0M1, Canada (e-mail: amin.banaie.92@gmail.com).

Manish Patel is with the Southern Company, Atlanta, GA 30308 USA (e-mail: MPATEL@southernco.com).

Color versions of one or more figures in this article are available at https://doi.org/10.1109/TPWRD.2022.3187223.

Digital Object Identifier 10.1109/TPWRD.2022.3187223

the requirement in Fig. 1, and if the phase currents hit their limit, $\Delta I_Q^{\pm}$ is reduced to bring the phase currents back to the acceptable range [3], [4]. Under this condition, $|I_P^+|$ would be considered zero. Conversely, if meeting the requirement in Fig. 1 does not violate the phase current limit, the difference between the maximum phase current and its limit determines the I_P^+ that can be generated using the straightforward and rather intuitive relations in [8]–[10], which will be elaborated in Section III.

This paper reveals why the above approach does not necessarily utilize the total current capacity of an IBR—that is, the ultimate objective of the LVRT provision. This paper also develops an algorithm to maximize both the active and reactive currents of an IBR while the reactive current is prioritized. We will prove that the path to prioritization and maximization of reactive current passes, ironically, through maximization of the active current first. As a result, the proposed solution will either prevent the aforementioned scaling of the $\Delta I_Q^{\pm}$ given by Fig. 1 or increase the scaling factor beyond what is offered by the state-of-the-art literature; hence maximizing the reactive currents as well. While the proposed approach fully complies with [3], [4], these GCs do not include any information about the possibility of such optimal reference currents for IBRs. By shedding light on this blind spot, the paper shows the feasibility of a significant increase in the power generated by the IBRs that meet [3], [4], highlighting the true value of the LVRT requirements in these GCs. The paper also presents a detailed comparative study between the proposed algorithm and the state-of-the-art literature on GC compliance. The problem formulation and solution presented in this paper are applicable to full-scale inverter-interfaced renewable energy sources, such as solar photovoltaic and Type IV wind farms.

II. Test System

PSCAD/EMTDC simulations of a modified version of the IEEE 39-bus system, depicted in Fig. 2, are used for this study [15]. The modifications include the addition of 16 IBRs to represent a grid with high penetration of renewable sources. The high number of IBRs also makes the impact of GC requirements more visible from a system-wide perspective. For the sake of simplicity, all IBRs are rated at 34.5 kV, 200 MW, and interfaced to the grid through 250-MVA, 230-kV/34.5-kV, YGd1 transformers. The phase current limit of all IBRs is $I_{\max} = 1.2$ pu.

III. Challenges in Effective Utilization of an IBR's Current Capacity

This section demonstrates the shortcomings of the common approach used in the literature to determine the reference for the positive-sequence active current of an IBR that generates negative-sequence current. When the reactive current is prioritized (as is the case in [3] and [4]), a straightforward way to derive the reference for $|I_P^+|$ is based on (1), which maintains the scalar sum of the positive- and negative-sequence current

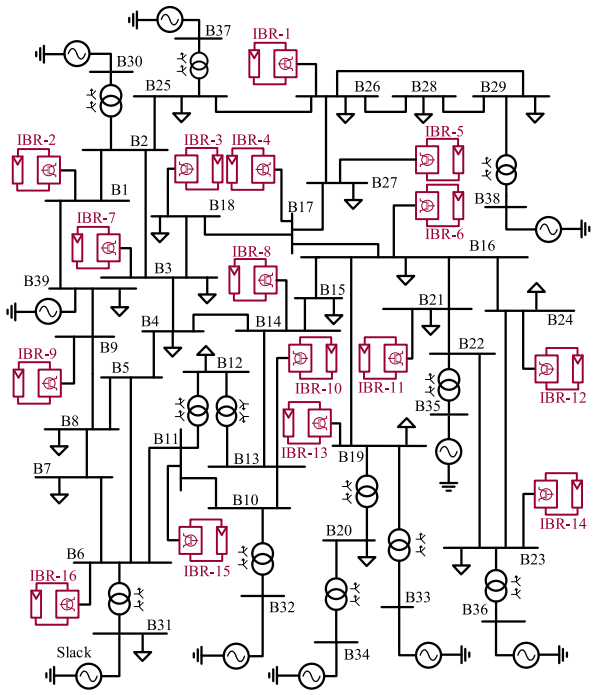

Fig. 2. Single-line diagram of the test system.

magnitudes below the phase current limit of the IBR [8], [9].

$$|I^+| + |I^-| = \sqrt{|I_P^+|^2 + |I_Q^+|^2} + \sqrt{|I_P^-|^2 + |I_Q^-|^2} \le I_{\max} \tag{1}$$

$|I_P^-|$ must be zero [3], [4], so the only unknown in (1) is $|I_P^+|$. The following case studies evaluate the performance of this approach.

A. Case 1

This case elaborates on the effective utilization of an IBR's current capacity when the ΔI_Q^+ and ΔI_Q^- given by Fig. 1 do not make the phase currents hit their limit. Consider IBR-4 of Fig. 2 during a bolted phase-B-to-phase-C (BC) fault at bus B27 at $t = 1$ s. The IBR's pre-fault current is 1 pu. The power factor is 1 at the point of measurement (POM), which is the high-voltage (HV) side of the main transformer [16]. The diagram of Fig. 1 is applied on the low-voltage (LV) side of the IBR's interface transformer, referred to as the point of connection (POC) [16]. Before the fault, $|I_Q^+| = 0.037$ pu (capacitive) and $|I_Q^-| = 0$ at the POC. The fault results in $\Delta V^+ = -0.192$ pu and $\Delta V^- = 0.177$ pu at the POC. Thus, $\Delta I_Q^+ = -0.480$ pu and $\Delta I_Q^- = 0.442$ pu for $K = 2.5$, resulting in $|I_Q^+| = 0.52$ pu and $|I_Q^-| = 0.44$ pu. Using these reactive currents and $I_{\max} = 1.2$ pu, the maximum $|I_P^+|$ given by (1) is 0.55 pu. These reference currents are met by the IBR quickly after the fault inception in Fig. 3(a). These measurements are taken from before the LC filter's shunt capacitor to focus only on the current of the inverter switches (although the capacitor's current is comparatively insignificant).

The phase currents resulting from the above sequence currents are displayed in Fig. 3(b). The maximum current is $|I_c| = 1.07$ pu, i.e., 65% of the IBR's 0.2-pu extra capacity for the LVRT

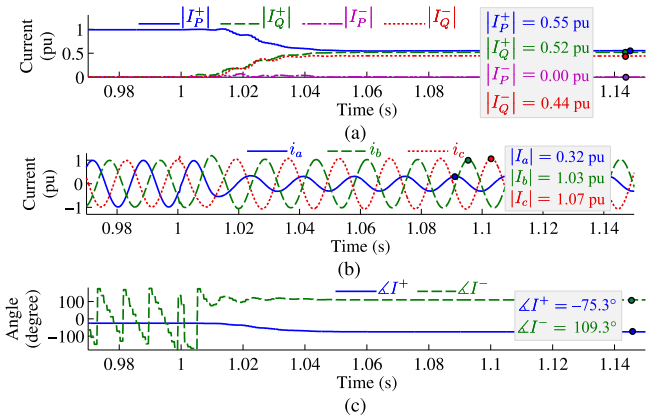

Fig. 3. Measurements for IBR-4 in Case 1, (a) Active and reactive sequence current magnitudes, (b) Instantaneous currents, (c) Sequence current angles.

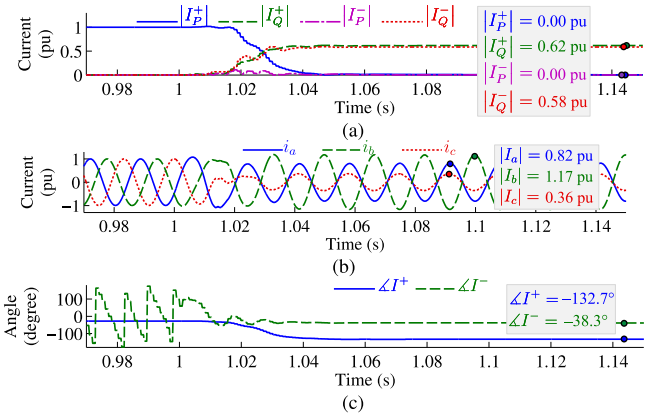

Fig. 4. Measurements for IBR-16 in Case 2, (a) Active and reactive sequence current magnitudes, (c) Instantaneous currents, (c) Sequence current angles.

current remains untapped. For phase B, 85% of this excess capacity remains unused. For phase A, this capacity is not used at all. This unused capacity stems from the scalar sum of (1), which is different from the vector sum that actually determines the phase currents. The underlying assumption of (1) is that I^+ and I^- are in phase. This assumption is invalid for most fault conditions, including the above fault (Fig. 3(c)). The 184.6° phase difference in Fig. 3(c) makes the vector sum of I^+ and I^- smaller than the scalar sum in (1), hence the inefficient utilization of the inverter's current capacity.

Since the maximum phase current, $|I_c|$, is 0.13 pu less than $I_{\max}$, one might expect that $|I_P^+|$ can be increased by at most 0.13 pu, and then the inverter's capacity is fully utilized. However, increasing $|I_P^+|$ by 0.13 pu while $|I_Q^+|$ and $|I_Q^-|$ are kept the same as in Fig. 3(a) results in $|I_a| = 0.41$ pu, $|I_b| = 1.15$ pu, $|I_c| = 1.13$ pu. These currents are still below the IBR's phase current limit. Here again, identification of reference currents based on scalar calculations causes the undesired result.

Although the GCs prioritize the reactive power, they also require maximizing active power [3], [4]. Effective utilization of the seemingly small 0.2-pu excess current capacity of the inverter in the phase domain offers sizable active power in the sequence domain. This can be made clear only when the excess current capacity is maximally used later in the paper.

B. Case 2

This case focuses on when the ΔI_Q^+ and ΔI_Q^- given by Fig. 1 make the phase currents hit their limit (which did not happen in Case 1). Consider IBR-16 when a phase-A-to-ground (AG) fault with $R_f = 5\,\Omega$ occurs at bus B7. For the pre-fault $|I_{Q\text{-pre}}^+| = 0.038$ pu (capacitive), $\Delta V^+ = -0.136$ pu, and $\Delta V^- = 0.136$ pu, the superimposed currents given for $K = 5$ by Fig. 1 yield $|I_Q^+| = 0.72$ pu and $|I_Q^-| = 0.68$ pu. The GCs permit lowering the active current to create room for these large reactive currents [3], [4]. However, even with zero active current, the reactive currents add up to 1.40 pu, violating the inequality in (1). Therefore, following the GC provisions mentioned in Section I, $|I_Q^+|$ and $|I_Q^-|$ are uniformly scaled down. The scaling factor that makes

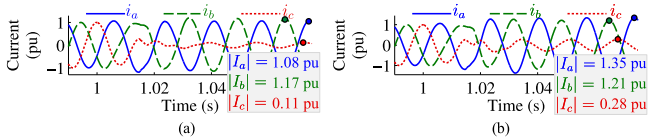

Fig. 5. Instantaneous phase currents of IBR-16 in Case 2, (a) Below the limit although injecting $|I_P^+|$, (b) Above the limit when injecting $|I_P^+|$.

$|I_Q^+|$ and $|I_Q^-|$ satisfy (1) is obtained by dividing the right side of (1) over 1.40 pu; i.e., $I_{\max}/1.40 = 0.857$. This would satisfy (1) by scaling down the reactive currents to their supposedly maximum values of $|I_Q^+| = 0.62$ pu and $|I_Q^-| = 0.58$ pu, which add up to 1.2 pu. Under this condition, it appears that the severity of the voltage drop has made the reactive currents required by the GC so large that no room is left to generate active current. These sequence currents, shown in Fig. 4(a), lead to the phase currents of Fig. 4(b). Phase B carries the largest current and is 0.03 pu less than $I_{\max}$.

One obvious problem of the above process is that the 0.857 scaling factor obtained using (1) prevents maximizing the reactive currents, and so 15% of the inverter's excess current capacity remains unused. If $|I_Q^+|$ and $|I_Q^-|$ were scaled down by a factor of 0.879 to 0.63 pu and 0.60 pu, respectively, then the current of phase C would reach to 1.2 pu. This would satisfy the IBR's phase current limit, even though it violates (1).

The second (and bigger) problem is not as obvious. It is taken for granted that once 0.879 is used to scale down $|I_Q^+|$ and $|I_Q^-|$ to 0.63 pu and 0.60 pu, and the phase C current hits the limit, no room is left to generate $|I_P^+|$ [6], [7], [10]. However, as shown in Fig. 5(a), the addition of a randomly chosen $|I_P^+| = 0.3$ pu (which amounts to 51.7 MW of active power) to $|I_Q^+| = 0.63$ pu and $|I_Q^-| = 0.60$ pu actually decreases the maximum phase current from 1.2 pu by 0.03 pu. Generation of another randomly chosen $|I_P^+| = 0.6$ pu, however, makes I_a and I_b larger than the limit (Fig. 5(b)). For such conditions, there is currently no solution in the literature to maximize $|I_P^+|$ without violating $I_{\max}$.

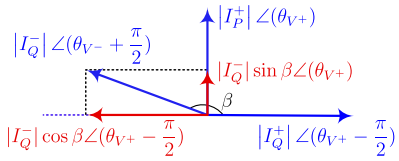

Fig. 6. Phasor diagram of the active and reactive sequence components of phase A current.

IV. Proposed Solution

This section presents, for the first time, an algorithm to comply with the GCs' requirement to maximize an IBR's active current during LVRT while the diagram of Fig. 1 is adhered to. This would address the challenges discussed in the last section using the following three-step process. While this section includes all of the information required to implement the proposed method, Section V will later elaborate on the reason behind the sequence of these three steps and why such information should ideally be included in the future revisions of any GC or IBR interconnection agreement that adopts the diagram in Fig. 1.

A. Step 1: Maximizing $|I_P^+|$ for the $|\Delta I_Q^\pm|$ of Fig. 1

The relation between the different components of an IBR's sequence currents and the phase currents that flow through the inverter switches is shown in (2) shown at the bottom of this page. where $\alpha = e^{j2\pi/3}$; θ_V denotes the voltage angle at the POC; pre in the subscript denotes the pre-LVRT quantities; and cap indicates the quantities associated with the shunt capacitor of the inverter's filter. From (2), the phase currents can be written as

$$I_\Phi = |I_Q^+|\angle\left(\theta_{V^+}-\frac{\pi}{2}+\varphi\right)+|I_P^+|\angle(\theta_{V^+}+\varphi) + |I_Q^-|\angle\left(\theta_{V^-}+\frac{\pi}{2}-\varphi\right) \tag{3}$$

where $\Phi \in \{a,b,c\}$, and φ is 0, $-2\pi/3$, and $2\pi/3$ for phases A, B, and C, respectively. The reactive components of I_Φ are derived using (4), which includes $\Delta I_Q^\pm$ given by Fig. 1.

$$|I_Q^+| = \left|\pm|I_{Q\text{-pre}}^+| + \Delta I_Q^+\right| - |I_{Q\text{-cap}}^+| \tag{4a}$$

$$|I_Q^-| = \Delta I_Q^- + |I_{Q\text{-cap}}^-| \tag{4b}$$

The objective is to find the active current $|I_P^+|$ in (3) such that the largest phase current given by this equation equals $I_{\max}$. Fig. 6 displays the three vectors on the right side of (3) for phase A, i.e., $\varphi = 0$. As shown in this figure, $|I_Q^+|\angle(\theta_{V^+}-\pi/2)$ and $|I_Q^+|\angle(\theta_{V^+})$ are 90° out of phase. Thus, they can generate two orthogonal coordinate axes onto which the third vector, i.e., $|I_Q^-|\angle(\theta_{V^-}+\pi/2)$, can be projected. In Fig. 6,

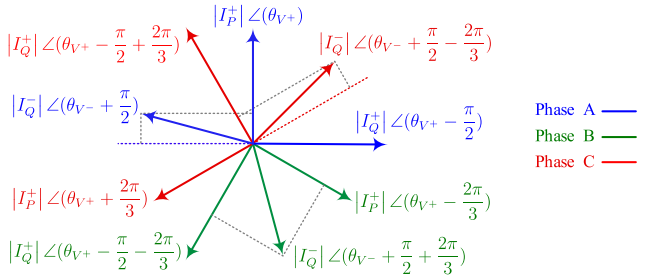

Fig. 7. Vector diagram of the active and reactive sequence components of phase currents.

$$\beta = \pi + \theta_{V^-} - \theta_{V^+} \tag{5}$$

β can be used to derive the red horizontal and vertical axis projections of $|I_Q^-|\angle(\theta_{V^-}+\pi/2)$ in Fig. 6 as $|I_Q^-|\cos\beta\angle(\theta_{V^+}-\pi/2)$ and $|I_Q^-|\sin\beta\angle(\theta_{V^+})$, respectively. Substituting $|I_Q^-|\angle(\theta_{V^-}+\pi/2)$ in (3) with these two projections, the current of phase A can be written as

$$I_a = (|I_Q^+|+|I_Q^-|\cos\beta)\angle\left(\theta_{V^+}-\frac{\pi}{2}\right) + (|I_P^+|+|I_Q^-|\sin\beta)\angle(\theta_{V^+}) \tag{6}$$

Therefore, the square magnitude of phase A current can be written as

$$|I_a|^2 = (|I_Q^+|+|I_Q^-|\cos\beta)^2+(|I_P^+|+|I_Q^-|\sin\beta)^2 \tag{7}$$

The above process must be done for all three phases. Fig. 7 shows the three vectors on the right side of (3) for all three phases. The dotted gray lines show how the negative-sequence reactive current of each phase is projected onto the two orthogonal axes of the positive-sequence active and reactive currents of the respective phase. By doing so, each phase current can be expressed as

$$I_\Phi = (|I_Q^+|+|I_Q^-|\cos(\beta+\varphi))\angle\left(\theta_{V^+}-\frac{\pi}{2}+\varphi\right) + (|I_P^+|+|I_Q^-|\sin(\beta+\varphi))\angle(\theta_{V^+}+\varphi) \tag{8}$$

The square magnitudes of the phase currents in (8) are

$$|I_\Phi|^2 = (|I_Q^+|+|I_Q^-|\cos(\beta+\varphi))^2+(|I_P^+|+|I_Q^-|\sin(\beta+\varphi))^2 \tag{9}$$

The IBR limit for the three phase currents can be expressed as the three inequalities embedded in (11) for different values of φ.

$$\begin{bmatrix} I_a \\ I_b \\ I_c \end{bmatrix} = \begin{bmatrix} 1 & 1 \\ \alpha^2 & \alpha \\ \alpha & \alpha^2 \end{bmatrix} \begin{bmatrix} \left|\pm|I_{Q\text{-pre}}^+| + \Delta I_Q^+\right|\angle\left(\theta_{V^+}-\frac{\pi}{2}\right)+|I_{Q\text{-cap}}^+|\angle\left(\theta_{V^+}+\frac{\pi}{2}\right)+|I_P^+|\angle(\theta_{V^+}) \\ \Delta I_Q^-\angle\left(\theta_{V^-}+\frac{\pi}{2}\right)+|I_{Q\text{-cap}}^-|\angle\left(\theta_{V^-}+\frac{\pi}{2}\right) \end{bmatrix} \tag{2}$$

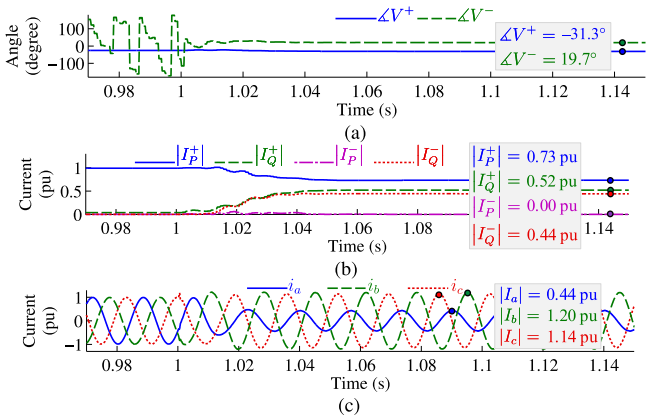

Fig. 8. Measurements for IBR-4 in Case 1, repeated using the proposed method, (a) Angles of the sequence voltages, (b) Active and reactive sequence current magnitudes at the POC, (b) Instantaneous currents of the switches.

$$|I_\Phi|^2 = (|I_Q^+| + |I_Q^-|\cos(\beta+\varphi))^2 + (|I_P^+| + |I_Q^-|\sin(\beta+\varphi))^2 \le I_{\max}^2 \qquad (10)$$

In (11), $|I_Q^+|$ and $|I_Q^-|$ are given by Fig. 1, and $|I_P^+|$ is the unknown. Solving these three inequalities yields three different ranges for $|I_P^+|$, each making the corresponding phase current less than $I_{\max}$. To maintain all phase currents below $I_{\max}$, the three inequalities must hold simultaneously. Thus, only the intersection of the three ranges is acceptable for $|I_P^+|$, resulting in (9) shown at the bottom of this page. In this relation, the first range stands for the obvious fact that $|I_P^+| \ge 0$. The second, third, and fourth ranges are the solutions of (11) for phases A, B, and C, respectively. If the intersection of the four ranges in (9) is not an empty set, the maximum active current is the upper bound of this intersection. Under such conditions, the GC is satisfied using only (9), and the further calculations of Sections IV-B and IV-C are not needed.

To show the difference made by the above process, consider the fault of Case 1 while IBR-4 uses (9) to determine $|I_P^+|$. Using the voltage angles in Fig. 8(a), $\beta = 231°$. Moreover, the LC filter's shunt capacitor generates $|I_{Q\text{-cap}}^+| = 0.031$ pu and $|I_{Q\text{-cap}}^-| = 0.008$ pu (not shown due to the space limitation). In addition, since there is no need to scale down the reactive currents and the fault conditions have not changed from Section III-A, $|I_Q^\pm|$ in Fig. 8(b) is similar to that in Fig. 3(a). Substituting these values into (4) and (9), the second, third, and fourth range for $|I_P^+|$ in (9) that correspond to phases A, B, and C are [–0.834, 1.531], [–1.574, 0.735], [–0.686, 0.828] pu, respectively. Thus, the maximum of the intersection of the four ranges in (9) is $|I_P^+| = 0.735$ pu, displayed in Fig. 8(b). The sequence currents in this figure satisfy both Fig. 1 and the GC requirement to maximize the IBR's active current, leading to an additional 28.3 MW of active power compared to Fig. 3. Furthermore, the phase currents through the inverter switches, depicted in Fig. 8(c), do not violate their limit.

B. Step 2: Scaling Down $|\Delta I_Q^\pm|$ of Fig. 1

This section and Section IV-C elaborate on (i) the conditions under which (9) returns an empty set, and (ii) the steps that must be taken in these conditions to satisfy the GC. An inverter's maximum current is fairly small. In addition, when a fault is not very far from the IBR and so the change in the voltage is significant, the reactive currents determined by Fig. 1 are quite large. The additional requirement for the negative-sequence current also increases the total reactive current by up to 100%. The small $I_{\max}$ and large $|I_Q^\pm|$ make it likely that one or more of the terms under the six radicals in (9) become negative. Since all of the formulations from (3) onwards are in the domain of real numbers, a negative term under even one radical in (9) would yield an unacceptable answer for $|I_P^+|$, i.e., $|I_P^+| \in \varnothing$. Even if all of the terms under the radicals in (9) are positive, it is still possible that the four ranges in (9) do not overlap, and $|I_P^+| \in \varnothing$. Under such conditions, at least one of the phase currents exceeds $I_{\max}$, because otherwise solving (11) and (9) would give $|I_P^+| = 0$, not $|I_P^+| \in \varnothing$.

When $I_{\max}$ is exceeded, the sequence reactive currents must be scaled down uniformly [3], [4]. The reference current generation schemes in the available literature scale the total positive- and negative-sequence reactive currents, $I_Q^\pm$ [6], [10]. Thus, the formulations in these schemes include scaling the pre-fault current, $I_{Q\text{-pre}}$, and the current through the capacitor of the inverter's LC filter, $I_{Q\text{-cap}}$, neither of which is actually controllable during LVRT. The following explains how the current should be scaled.

When the reactive currents are not scaled down, the following relation holds as long as the same $K-$factor is used for the

$$|I_P^+| \in \Bigg(\mathbb{R}^{\ge 0} \cap \left[-\sqrt{I_{\max}^2 - (|I_Q^+| + |I_Q^-|\cos\beta)^2} - |I_Q^-|\sin\beta,\ \sqrt{I_{\max}^2 - (|I_Q^+| + |I_Q^-|\cos\beta)^2} - |I_Q^-|\sin\beta \right]$$
$$\cap \left[-\sqrt{I_{\max}^2 - \left(|I_Q^+| + |I_Q^-|\cos\left(\beta - \frac{2\pi}{3}\right)\right)^2} - |I_Q^-|\sin\left(\beta - \frac{2\pi}{3}\right),\ \sqrt{I_{\max}^2 - \left(|I_Q^+| + |I_Q^-|\cos\left(\beta - \frac{2\pi}{3}\right)\right)^2} - |I_Q^-|\sin\left(\beta - \frac{2\pi}{3}\right) \right]$$
$$\cap \left[-\sqrt{I_{\max}^2 - \left(|I_Q^+| + |I_Q^-|\cos\left(\beta + \frac{2\pi}{3}\right)\right)^2} - |I_Q^-|\sin\left(\beta + \frac{2\pi}{3}\right),\ \sqrt{I_{\max}^2 - \left(|I_Q^+| + |I_Q^-|\cos\left(\beta + \frac{2\pi}{3}\right)\right)^2} - |I_Q^-|\sin\left(\beta + \frac{2\pi}{3}\right) \right] \Bigg) \qquad (11)$$

positive and negative sequence in Fig. 1.

$$\frac{\Delta I_Q^+}{\Delta I_Q^-} = \frac{\Delta V^+}{\Delta V^-} \tag{12}$$

Therefore, the IBR's equivalent impedances in the two sequence circuits are similar, replicating a synchronous generator. An IBR should ideally maintain the same relation after the currents are scaled down, so that the similarity with the synchronous generators is preserved. Scaling the total reactive currents violates (12) since the total reactive currents are not limited to only the superimposed currents given by Fig. 1. Therefore, only $\Delta I_Q^{\pm}$ must be scaled down in the derivations that yield the scaling factor, ρ. To calculate this factor, $\Delta I_Q^{\pm}$ and I_P^+ in (2) are set to $\rho\Delta I_Q^{\pm}$ and 0, respectively, resulting in

$$\begin{bmatrix} I_a \\ I_b \\ I_c \end{bmatrix} = \begin{bmatrix} 1 & 1 \\ \alpha^2 & \alpha \\ \alpha & \alpha^2 \end{bmatrix} \times \begin{bmatrix} \left(\left| \pm |I_{Q\text{-pre}}^+| + \rho\Delta I_Q^+ \right| - |I_{Q\text{-cap}}^+| \right) \angle \left(\theta_{V^+} - \frac{\pi}{2} \right) \\ (\rho\Delta I_Q^- + |I_{Q\text{-cap}}^-|) \angle \left(\theta_{V^-} + \frac{\pi}{2} \right) \end{bmatrix} \tag{13}$$

This equation must be solved for ρ such that $\max\{|I_a|, |I_b|, |I_c|\} = I_{\max}$ to ensure maximum utilization of the inverter's capacity.

Equating the square magnitudes of the phase currents given by (13) with $I_{\max}^2$ yields the three equations embedded in (14) shown at the bottom of this page. In this equation, $\varphi = 0, -2\pi/3$, and $+2\pi/3$, correspond to phases A, B, and C, respectively. This relation can be written with respect to ρ, as in

$$I_{\max}^2 = \lambda_{2\varphi}\rho^2 + \lambda_{1\varphi}\rho + \lambda_{0\varphi} \tag{15}$$

where the coefficients $\lambda_{2\varphi}$, $\lambda_{1\varphi}$, and $\lambda_{0\varphi}$ must be calculated. To this end, the terms with equal powers of ρ have to be calculated after (14) is expanded. In this expansion, the possibility of both positive and negative $|I_{Q\text{-pre}}^+|$ and the presence of the absolute value operator in $|\pm|I_{Q\text{-pre}}^+| + \rho\Delta I_Q^+|$ should be considered. For a capacitive pre-fault reactive current, the expression inside the absolute value operator, i.e., $-|I_{Q\text{-pre}}^+| + \rho\Delta I_Q^+$, is negative, so $|-|I_{Q\text{-pre}}^+| + \rho\Delta I_Q^+| = |I_{Q\text{-pre}}^+| - \rho\Delta I_Q^+$. For inductive pre-fault reactive current, however, the expression inside the absolute value operator, i.e., $|I_{Q\text{-pre}}^+| + \rho\Delta I_Q^+$ is either positive or negative—i.e., $||I_{Q\text{-pre}}^+| + \rho\Delta I_Q^+|$ is either $|I_{Q\text{-pre}}^+| + \rho\Delta I_Q^+$ or $-|I_{Q\text{-pre}}^+| - \rho\Delta I_Q^+$, depending on the sign of $|I_{Q\text{-pre}}^+| + \rho\Delta I_Q^+$. Since both the positive and negative signs must be considered for $|I_{Q\text{-pre}}^+|$ in $|\pm|I_{Q\text{-pre}}^+| + \rho\Delta I_Q^+|$, this expression can theoretically take four distinct values, out of which only one is valid for a given LVRT condition. All these four possibilities must be considered in the expansion of (14). By doing so, the coefficients $\lambda_{2\varphi}$, $\lambda_{1\varphi}$, and $\lambda_{0\varphi}$ can be as expressed in (16), shown at the bottom of the next page. The introduction of a new binary variable, μ, and using $\pm$ and $\mp$ signs make this equation applicable to all four possibilities. if $I_{Q\text{-pre}}^+$ is capacitive, $\mu = -1$, and the upper sign must be used in $\pm$ and $\mp$. For an inductive $I_{Q\text{-pre}}^+$, however, the lower sign must be used in $\pm$ and $\mp$, and $\mu = -1$ when $|I_{Q\text{-pre}}^+| + \rho\Delta I_Q^+ < 0$, and $\mu = 1$ when $|I_{Q\text{-pre}}^+| + \rho\Delta I_Q^+ > 0$. As ρ is the unknown of (15), the sign of $|I_{Q\text{-pre}}^+| + \rho\Delta I_Q^+$ cannot be determined before (15) is solved. Thus, (15) must be solved for both conditions, i.e., $|I_{Q\text{-pre}}^+| + \rho\Delta I_Q^+ < 0$ and $|I_{Q\text{-pre}}^+| + \rho\Delta I_Q^+ > 0$. For each of these inequalities, the calculated ρ is acceptable if the respective inequality is held for that ρ.

To find the optimal ρ that satisfies all of the constraints, one should note that the equation for each phase embedded in (15) is solved independently of the other two equations in (15) (for the other two phases) but the constraint on the current magnitude must be satisfied for all three phases. Therefore, the scaling factor can be found by, first, finding all of the possible solutions for ρ in each equation embedded in (15); then, discarding any ρ that is outside the [0, 1] range because such ρ's do not scale down the current magnitude; then, choosing the largest ρ that is the solution of (15) for one of the phases but also simultaneously keeps the current magnitude in the other two phases below $I_{\max}$.

C. Step 3: Maximizing $|I_P^+|$ After Scaling Reactive Currents

Since (13) was solved to satisfy the $\max\{|I_a|, |I_b|, |I_c|\} = I_{\max}$ condition, the scaled-down positive- and negative-sequence reactive currents obtained in Step 2 make the current of at least one phase equal to the inverter's limit. When one of the phase currents reaches the limit, it might seem natural that the inverter has no room to inject active current, as it has been assumed so in various studies, e.g., [6], [7], [10], and [11]. The following formulation attempts to calculate non-zero positive-sequence active current, I_P^+, while the reactive currents obtained in Step 2 remain intact and the inverter's phase current limit is satisfied.

Assume, without loss of generality, that $|I_a|$ is the largest phase current at the end of Step 2 when $I_Q^{\pm}$ is scaled down and no I_P^+ is generated, i.e.,

$$|I_a| = \left| |I_Q^+| \angle \left(\theta_{V^+} - \frac{\pi}{2} \right) + |I_Q^-| \angle \left(\theta_{V^-} + \frac{\pi}{2} \right) \right| = I_{\max} \tag{17}$$

The angle between I_Q^+ and I_Q^- in (17) is β defined in (5). Either $0 \le \beta \le \pi$, as in Fig. 9(a), or $\pi < \beta < 2\pi$, as in Fig. 9(b)

$$I_{\max}^2 = \left(\left| \pm |I_{Q\text{-pre}}^+| + \rho\Delta I_Q^+ \right| - |I_{Q\text{-cap}}^+| \right)^2 + (\rho\Delta I_Q^- + |I_{Q\text{-cap}}^-|)^2 + 2 \left(\left| \pm |I_{Q\text{-pre}}^+| + \rho\Delta I_Q^+ \right| - |I_{Q\text{-cap}}^+| \right) \times (\rho\Delta I_Q^- + |I_{Q\text{-cap}}^-|) \cos(\beta + \varphi) \tag{14}$$

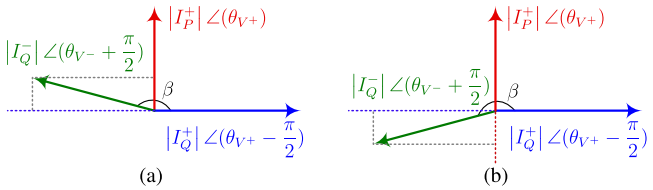

Fig. 9. Two possible situations for phase A sequence components depending on β, (a) $0 \le \beta \le \pi$, (b) $\pi < \beta < 2\pi$.

(Section V-C will elaborate on the probability of each of these conditions in practical power systems). The following analyzes both of the conditions in Fig. 9. When I_P^+ is not generated, by projecting I_Q^- onto the axes made by I_Q^+ and its orthogonal axis (which is the axis of the respective I_P^+ if I_P^+ were generated), $|I_a|$ can be written as

$$|I_a| = I_{\max} = \sqrt{|I_x|^2 + |I_y|^2} \tag{18}$$

where

$$I_x = (|I_Q^+| + |I_Q^-|\cos\beta)\angle\left(\theta_{V^+} - \frac{\pi}{2}\right) \tag{19a}$$

$$I_y = (|I_Q^-|\sin\beta)\angle\theta_{V^+} \tag{19b}$$

For Fig. 9(a), in which $\sin\beta \ge 0$, I_y and $|I_p^+|\angle\theta_{V^+}$ are in phase. Therefore, generating any $|I_p^+|\angle\theta_{V^+}$ in this case increases $|I_y|$ and pushes $|I_a|$ beyond the $I_{\max}$ limit considered in (17). Thus, the IBR cannot generate I_P^+ when $0 \le \beta \le \pi$.

For $\pi \le \beta \le 2\pi$ in Fig. 9(b), however, $\sin\beta < 0$, and so I_y and $|I_p^+|\angle\theta_{V^+}$ are 180° out of phase. Thus, an active current as large as

$$|I_P^+| = -2|I_Q^-|\sin\beta \tag{20}$$

can be generated. This would keep $|I_y|$ unchanged because for the $|I_P^+|$ given by (20), $I_y = (|I_Q^-|\sin\beta - 2|I_Q^-|\sin\beta)\angle\theta_{V^+} = -|I_Q^-|\sin\beta\angle\theta_{V^+}$. When $|I_y|$ and $|I_x|$ in (18) do not change, $|I_a|$ is maintained at $I_{\max}$. However, there is no guarantee that I_b and I_c remain below $I_{\max}$ after injecting the I_P^+ given by (20).

Although the above formulation does not ensure that I_b and I_c are less than $I_{\max}$, it proves that (9) can be used again to determine the $|I_P^+|$ that can be generated after scaling down $I_Q^\pm$ in Step 2. Substituting the $I_{\max}$ given by (18) and (19) into (9) shows that the $|I_P^+|$ given by (20) is, in fact, the upper bound of the second range on the right side of (9), which corresponded to phase A in the derivations of Section IV-A. It can be similarly proved that if the derivations in (17)–(20) are carried out for phases B and C (which would require only shifting β by $+2\pi/3$ and $-2\pi/3$, respectively), substituting the $I_{\max}$ given by (18) and (19) into (9) makes the upper bound

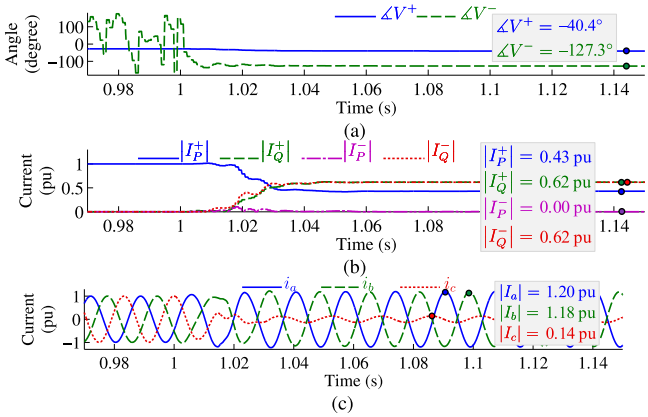

Fig. 10. Measurements for IBR-16 in Case 2, repeated using the proposed method, (a) Angles of the sequence voltages, (b) Active and reactive sequence current magnitudes, (d) Instantaneous currents.

of the third and the fourth range on the right side of (9) equal to the $|I_P^+|$ in (20), respectively. The third and the fourth range in (9) corresponded to phases B and C in the derivations of Section IV-A, respectively. Consequently, if the scaled-down reactive current calculated in Step 2 are plugged into (9) as $I_Q^\pm$, this equation will provide the maximum $|I_P^+|$ that keeps all of the phase currents below $I_{\max}$.

The algorithm developed in this section can be summarized as Step 1:

- Calculate $\Delta I_Q^\pm$ in Fig. 1 using the measured $\Delta V^\pm$ and the given K-factor.
- Calculate $|I_Q^\pm|$ using (4), β using (5), and $|I_P^+|$ using (9).
- If $|I_P^+| \in \varnothing$, proceed to Step 2; otherwise, no further action is needed and the references are $|I_Q^\pm|$ and $|I_P^+|$ given by (4) and (9), respectively.

Step 2:

- Find $\lambda_{2\varphi}$, $\lambda_{1\varphi}$, and $\lambda_{0\varphi}$ using (16).
- Find ρ in (15).
- Set $|I_Q^+| = |\pm|I_{Q\text{-pre}}^+| + \rho\Delta I_Q^+| - |I_{Q\text{-cap}}^+|$ and $|I_Q^-| = \rho\Delta I_Q^- + |I_{Q\text{-cap}}^-|$.

Step 3:

- Calculate $|I_P^+|$ using (9).

The derivations in Sections IV-B and IV-C whenever (9) does not return a non-zero $|I_P^+|$, which is a wide range of LVRT conditions. Consider, for example, the previously-studied Case 2 when IBR-16 implements the proposed method. From Section III-B, $|I_{Q\text{-pre}}^+|$ =0.038 pu (capacitive), ΔI_Q^+ =0.68 pu, and ΔI_Q^- =0.68 pu. The angles of the sequence voltages in Fig. 10(a) give $\beta = 93.1°$. For the filter's capacitor, $|I_{Q\text{-cap}}^+|$ =0.035 pu and

$$\lambda_{2\varphi} = (\Delta I_Q^+)^2 + 2\mu\Delta I_Q^+\Delta I_Q^-\cos(\beta+\varphi) + (\Delta I_Q^-)^2 \tag{16a}$$

$$\lambda_{1\varphi} = 2\Delta I_Q^+|I_{Q\text{-cap}}^+| \pm 2\mu|I_{Q\text{-pre}}^+|\Delta I_Q^+ + 2\Delta I_Q^-|I_{Q\text{-cap}}^-| + (\mp 2\mu|I_{Q\text{-pre}}^+|\Delta I_Q^- + 2\mu\Delta I_Q^+|I_{Q\text{-cap}}^-| - 2|I_{Q\text{-cap}}^+|\Delta I_Q^-)\cos(\beta+\varphi) \tag{16b}$$

$$\lambda_{0\varphi} = |I_{Q\text{-pre}}^+|^2 \pm 2\mu|I_{Q\text{-pre}}^+||I_{Q\text{-cap}}^+| + |I_{Q\text{-cap}}^+|^2 + |I_{Q\text{-cap}}^-|^2 + (\mp 2\mu|I_{Q\text{-pre}}^+||I_{Q\text{-cap}}^-| - 2|I_{Q\text{-cap}}^+||I_{Q\text{-cap}}^-|)\cos(\beta+\varphi) \tag{16c}$$

$|I^-_{Q\text{-cap}}|$ =0.005 pu. Substituting these values into (4) and then (9) makes the term under the radical in the third range on the right side of (9) (corresponding to phase B) negative. Thus, $|I^+_P|$ cannot be found in the first step, and the reactive currents must be scaled down.

Substituting the above values into (16), the coefficients $(\lambda_{2,\varphi}, \lambda_{1,\varphi}, \lambda_{0,\varphi})$ of the quadratic (15) for phases A, B, and C (corresponding to $\varphi = 0$, $-2\pi/3$, and $+2\pi/3$) will be (0.8748, 0.0103, 0.0000), (1.7495, 0.0206, 0.0000), and (0.1501, 0.0018, 0.0000), respectively. Solving the three quadratic equations in (15), the solutions for ρ will be (–1.2889, 1.2771), (–0.9131,0.9014), and (–3.1035, 3.0917), for $\varphi = 0$, $-2\pi/3$, and $+2\pi/3$ associated with phases A, B, and C, respectively. Among these values, ρ =0.9014 is a solution of (15) for phase B inside the [0, 1] range. For this ρ, the scaled-down current references on the right side of (13) are $|I^+_Q| = |-|I^+_{Q\text{-pre}}| + \rho\Delta I^+_Q| - |I^+_{Q\text{-cap}}|$ =0.62 pu, and $|I^-_Q| = \rho\Delta I^-_Q + |I^-_{Q\text{-cap}}|$ =0.62 pu. When these reference currents are plugged into (13), the current of phase B is limited to $I_{\max}$=1.2 pu while the current of the other two phases are smaller than the limit ($|I_a|$ =0.85 pu and $|I_c|$ =0.35 pu). Thus, ρ =0.9014 is the acceptable scaling factor.

Since the current of phase B is maximum, the IBR will be able to generate I^+_P if $180^\circ < \beta - 120^\circ < 360^\circ$. $\beta = 93.1^\circ$, and so this condition holds. Using the above $I^\pm_Q$, the largest $|I^+_P|$ that satisfies (9) is 0.43 pu, displayed along with $|I^\pm_Q|$ in Fig. 10(b). As shown in Fig. 10(c), this additional active current keeps the phase currents below $I_{\max}$; it just changes the maximum current from phase B (at the end of Step 2) to phase A ($|I_a|$ =1.2 pu in in Fig. 10(c)). From the perspective of LVRT performance of the IBR, the impact of this I^+_P is profound: it leads to the generation of 74.7 MW of active power by IBR-4, while the inverter control schemes available in the literature (such as [6], [7], and [10]) offer zero active power for this fault scenario.

V. Discussion

The formulations derived in the last section are sufficient to implement the proposed method. This section presents further insight into this solution, including its superiority in the generation of reactive current, justification for the sequence of steps taken in this solution, and the probability of generating non-zero active current in practical power systems.

A. Reactive Currents Improvement by the Proposed Method

This section demonstrates that the advantages of the proposed method are not limited to only the increased active current generation discussed in Section IV. This method maximizes also the inverter's reactive current beyond the levels given by existing techniques. In the available literature for GC compliance of IBRs, when the ΔI^+_Q and ΔI^-_Q given by Fig. 1 make the phase currents exceed $I_{\max}$, the scaling factor for $\Delta I^\pm_Q$ is obtained by dividing $I_{\max}$ over the estimated maximum phase current caused by the $\Delta I^\pm_Q$ of Fig. 1 [8], [10]. In the state-of-the-art literature, such as [8] and [9], this estimate is obtained based on (1) and is the scalar sum of $|I^+|$ and $|I^-|$. However, the phase current is actually the sum of I^+ and I^- (for each phase). The phase angle between I^+ and I^- makes the scalar sum used in the available literature larger than $I^+ + I^-$, causing a smaller scaling factor. This would, in turn, make the reactive current generated by existing techniques smaller. The proposed method, however, estimates the maximum phase current correctly through the vector sum of sequence currents and calculates the scaling factor using (13) to (16). This can result in noticeably larger reactive currents. The following case study illustrates this issue.

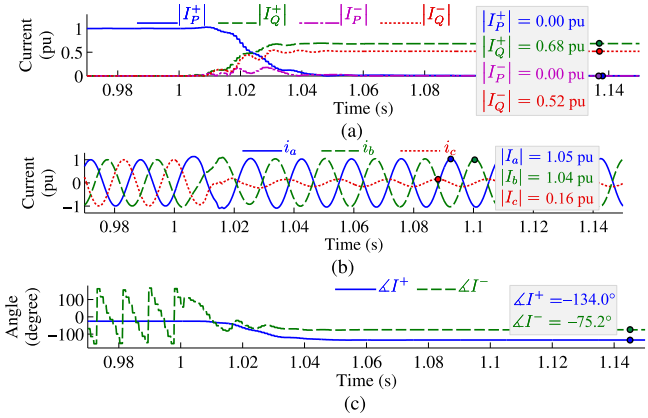

Fig. 11. Measurements for IBR-4 in Case 3 using the method of [8], [9], (a) Active and reactive sequence current magnitudes, (b) Instantaneous currents, (c) Angles of the sequence currents.

1) Case 3: Consider IBR-4 implements existing methods, such as [8] and [9], during a bolted AG fault at B16. For this case, $K = 6$, $|I^+_{Q\text{-pre}}|$ =0.038 pu, $\Delta V^+ = -0.199$ pu, and ΔV^- =0.155 pu, and so the sequence reactive current references are $|I^+_Q| = 1.23$ pu and $|I^-_Q| = 0.93$ pu. The maximum phase current estimated by (1) will be 2.16 pu, which violates the 1.2 pu limit. Thus, the reference currents are scaled down by a factor of $I_{\max}/2.16 = 0.555$ to obtain $|I^+_Q| = 0.68$ pu and $|I^-_Q| = 0.52$ pu shown in Fig. 11(a). The maximum of the resultant phase currents in Fig. 11(b) is $|I_a| = 1.05$ pu.

If IBR-4 adopts the proposed method, i.e., by substituting $|I^+_Q| = 1.23$ pu, $|I^-_Q| = 0.93$ pu, $|I^+_{Q\text{-cap}}|$ =0.033 pu, and $|I^-_{Q\text{-cap}}|$ =0.004 pu, along with sequence voltage angles of Fig. 12(a) in (4) and (9), the terms under the radicals in the first and third ranges on the right side of (9) (corresponding to phases A and C) become negative. Thus, $|I^+_P|$ cannot be found in Step 1, and the reactive currents must be scaled down. Calculating the coefficients $(\lambda_{2,\varphi}, \lambda_{1,\varphi}, \lambda_{0,\varphi})$ from (16) and solving (15), the solutions for ρ will be –0.6524 and 0.6439 for phase A, –0.6576 and 0.6491 for phase B, and –4.5768 and 4.5691 for phase C. Two of these solutions, i.e., 0.6439 and 0.6491 are inside the [0,1] range. However, $\rho = 0.6491$ yields $|I_a|$ =1.21 pu, $|I_b|$ =1.20 pu, and $|I_c|$ =0.17 pu and so makes the phase A current exceed the limit. The acceptable solution is, therefore, $\rho = 0.6439$, for which the sequence currents are $|I^+_Q| = |-|I^+_{Q\text{-pre}}| + \rho\Delta I^+_Q| - |I^+_{Q\text{-cap}}|$ =0.77 pu, and $|I^-_Q| = \rho\Delta I^-_Q + |I^-_{Q\text{-cap}}|$ =0.60 pu. Note that $\beta = 59.2^\circ$ for this case, and the condition for generating extra $|I^+_P|$ in Section IV-C does not hold. This would result in the sequence currents of Fig. 12(b), which yield the phase currents of Fig. 12(c). A

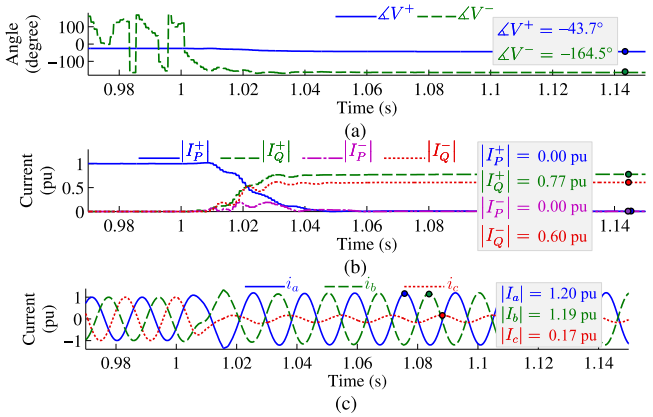

Fig. 12. Measurements for IBR-4 in Case 3 using the proposed method, (a) Angles of the sequence voltages, (c) Active and reactive sequence current magnitudes, (d) Instantaneous currents.

comparison between Figs. 11(a) and 12(b) reveals the advantage of the proposed method, which results in the generation of an additional 16 MVAr reactive power.

B. Sequence of Steps

The following explains the rationale behind the order of the steps taken in Section IV. Since the GCs prioritize reactive current over active current during LVRT, it might be naturally presumed (as has been done in [6] and [11]) that the order of the steps taken to satisfy the GCs' LVRT requirement should plausibly be: first, checking if the reactive currents given by Fig. 1 increase the phase currents beyond the $I_{\max}$ limit. Only if this limit is not violated, a non-zero active current is calculated/generated. Otherwise, no attempt is made to generate an active current, as the IBR has supposedly no extra capacity left, and even the pair of reactive currents given by Fig. 1 needs to be scaled down.

Conversely, the algorithm proposed in Section IV first attempts to find the maximum active current for the reactive currents of Fig. 1 without examining whether these reactive currents cause unacceptably large phase currents. Only afterwards are the reactive currents scaled down if need be. This might seem counterintuitive given the requirement to prioritize reactive currents. However, the irony is that for the very purpose of prioritizing/maximizing reactive currents, it is necessary to examine the possibility of generating active current before a potential scale-down of reactive currents. This stems from the fact that, depending on the magnitudes/angles of the sequence currents, there may occur a condition in which the non-scaled $I_Q^{\pm}$ of Fig. 1 (without any I_P^{+}) make the phase currents exceed $I_{\max}$, while the addition of a properly chosen I_P^{+} can bring the phase currents below $I_{\max}$ without the need to scale down the reactive currents given by Fig. 1. Such a scenario is depicted for the phase A current in Fig. 13. The phase current derived from the sum of I_Q^{-} and I_Q^{+}, $I_a^{(1)}$, exceeds the $I_{\max}$ limit. However, this figure shows that the addition of I_P^{+} places the phase current

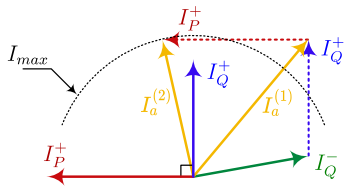

Fig. 13. Phasor diagram relating $I_{\max}$ to sequence active and reactive currents.

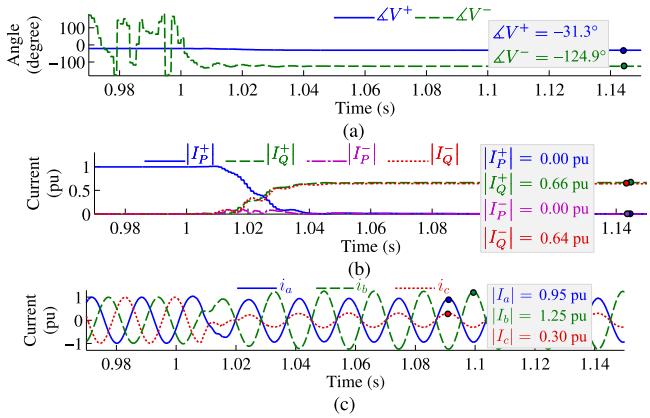

Fig. 14. Measurements for IBR-14 in Case 4 without active current generation, (a) Active and reactive sequence current magnitudes, (c) Instantaneous currents, (d) Angles of the sequence voltages.

($I_a^{(2)}$) within the acceptable range without reducing the reactive currents.

The GCs allow scaling down $I_Q^{\pm}$ only if it is necessary to do so, which is not the case for conditions like the one displayed in Fig. 13. Thus, the above sequence of steps is pivotal for satisfying [3], [4]. The following case study shows how the sequence of steps for calculating the inverter currents impacts the GC compliance.

1) Case 4: Consider an AG fault with $R_f = 5\ \Omega$ at 40% of the line connecting B23 to B24 in Fig. 2. For IBR-14, $\Delta V^{+} = -0.109$ pu and $\Delta V^{-} = 0.106$ pu, and so the superimposed reactive currents in Fig. 1 will be $\Delta I_Q^{+} = -0.65$ pu and $\Delta I_Q^{-} = -0.64$ pu for $K = 6$. Before the fault, the power factor of this IBR is 1 at the POM, which makes the pre-fault reactive current at the POC $|I_{Q\text{-pre}}^{+}| = 0.038$ pu. The POC voltage can be used to calculate $|I_{Q\text{-cap}}^{+}| = 0.037$ pu and $|I_{Q\text{-cap}}^{-}| = 0.003$ pu for the shunt capacitor of the inverter's filter. Therefore, the reactive current references given by (4) are $|I_Q^{+}| = 0.66$ pu and $|I_Q^{-}| = 0.64$ pu. Using the sequence voltage angles shown in Fig. 14(a), the angles of I_Q^{+} and I_Q^{-} are –121.3° and –34.9°, respectively. If the IBR generates these reactive currents, with no active current, as in Fig. 14(b), the current of phase B will exceed the limit in Fig. 14(c). If the sequence of steps used by the proposed method is not applied, the only way to bring the phase current within the acceptable range is to scale down $I_Q^{\pm}$ by 96%; i.e., sub-optimal reactive currents and zero active current.

Meanwhile, if the reactive currents and sequence voltage angles shown in Fig. 14(b) and 14(c) are plugged into (9),

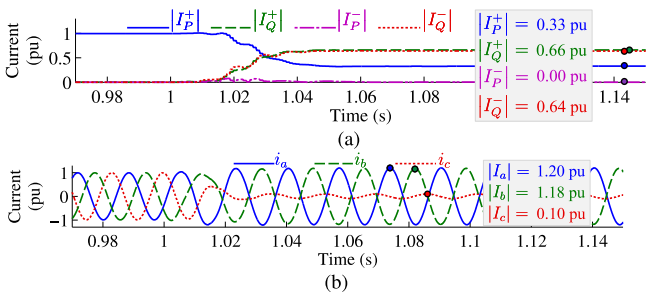

Fig. 15. Measurements for IBR-14 in Case 4 with the proposed method, (a) Active and reactive sequence current magnitudes, (c) Instantaneous currents.

the $|I_P^+|$ generated by the inverter becomes 0.33 pu. Using the sequence voltage angles of Fig. 14(c), the angle of I_P^+ is –31.3°. The angle between this I_P^+ and the above-mentioned reactive currents brings $|I_b|$ below $I_{\max}$ and makes $|I_a|$ equal to $I_{\max}$ (Fig. 15). Therefore, the phase current limit is satisfied without reducing reactive currents and with generating maximum active current; i.e., full compliance with [3] and [4]. Similar to the case at the end of Section IV, the active power generated by the IBR is huge and exceeds 60 MW.

C. Probability of Finding Non-Zero $|I_P^+|$ in Step 3

Section IV-C proved that an IBR can generate non-zero $|I_P^+|$ after $I_Q^\pm$ are scaled down only if $\beta + \varphi$ is inside the $[180°, 360°]$ range, where φ is 0, $+120°$, or $-120°$ when the maximum phase current after scaling down $I_Q^\pm$ occurs in phase A, phase B, or phase C, respectively. This section investigates the likelihood of $180° < (\beta + \varphi) < 360°$ in real power systems. As explained below, this analysis depends on the fault type.

1) Single-Phase-to-Ground-Faults: For a bolted AG fault, the phase lead of the negative-sequence voltage over the positive-sequence voltage ($\theta_{V^-} - \theta_{V^+}$) is about 180°. This angle progresses in the counterclockwise direction as the fault resistance increases, but the progression does not exceed $60° \sim 70°$ even for very large fault resistances (refer to Fig. 10 in [17]). Thus, $\theta_{V^-} - \theta_{V^+}$ is inside the [180°, 240°] range at an IBR's POM. Assuming a YNd1 interface transformer for the IBR, θ_{V^-} and θ_{V^+} shift by $+30°$ and $-30°$ when moving from the POM to the POC, and so the β (defined in (5)) measured at the POC is normally inside [60°, 120°] for AG faults and YNd1 transformer.

In the meantime, the phase lead of the negative-sequence reactive current over the positive-sequence reactive current, $\angle I_Q^- - \angle I_Q^+$, obtained through (13), is β, $\beta - 120°$, and $\beta + 120°$, for phases A, B, and C, respectively. Given the above range for β, the following angles are obtained at the POC:

- $60° < \angle I_Q^- - \angle I_Q^+ < 120°$ for phase A,
- $-60° < \angle I_Q^- - \angle I_Q^+ < 0°$ for phase B, and
- $180° < \angle I_Q^- - \angle I_Q^+ < 240°$ for phase C.

The smaller angle between the two sequence components of phase B current makes $|I_b|$ larger than the phase A and C currents and equal to $I_{\max}$ in Step 2 (as observed in the case study at the end of Section IV-C). As mentioned earlier, when $|I_b| = I_{\max}$, the IBR is able to generate $|I_P^+|$ in Step 3 if $180° < \beta - 120° < 360°$. This condition is normally satisfied as the above discussion indicated that β is inside [60°, 120°] for AG faults.

For a YNd11 transformer, θ_{V^-} and θ_{V^+} shift by $-30°$ and $+30°$, respectively, when moving from the POM to the POC, and so normally $-60° < \beta < 0°$ at the POC during AG faults. This makes the angle between I_Q^+ and I_Q^- minimum for phase A, hence $|I_a| = I_{\max}$ in Step 2. Thus, the IBR can generate $|I_P^+|$ in Step 3 if $180° < \beta < 360°$. This condition normally holds since $-60° < \beta < 0°$. A similar analysis and conclusion can be made for phase-B- and phase-C-to-ground faults as well.

2) Double-Phase-Faults: For BC and BCG faults, $\theta_{V^-} - \theta_{V^+}$ at the POM is close to zero [17]. It can be proven that as the fault location moves farther from the IBR, intermediate infeed currents with active component in the path between the IBR and the fault location makes $\theta_{V^-} - \theta_{V^+}$ retard into the fourth quadrant. The active intermediate infeed currents are generated by the other IBRs and synchronous generator-based sources (the latter of which has a greater impact due to its higher fault current magnitude). As a result, $\theta_{V^-} - \theta_{V^+}$ tilts towards the [−60°, 0°] range at the POM [17]. Considering the ±30° phase shifts introduced by a YNd1 transformer, β given by (5) is in the [180°, 240°] range at the POC. Using (13), this range for β leads to

- $180° < \angle I_Q^- - \angle I_Q^+ < 240°$ for phase A,
- $60° < \angle I_Q^- - \angle I_Q^+ < 120°$ for phase B, and
- $-60° < \angle I_Q^- - \angle I_Q^+ < 0°$ for phase C.

The angle between I_Q^+ and I_Q^- is smaller for phase C, indicating that the current of phase C is maximum and equal to $I_{\max}$ at the end of Step 2. As mentioned in Section IV-C, when the phase C current is maximum, an IBR can generate I_P^+ if $180° < \beta + 120° < 360°$. Meanwhile, it was shown in the above that $180° < \beta < 240°$, and so $300° < \beta < 360°$. Thus, the condition on β to generate I_P^+ in Step 3 holds.

If the transformer's vector group is YNd11, β at the POC is normally inside [60°, 120°] for BC and BCG faults. This makes $|I_b|$ equal to $I_{\max}$ in Step 2. Thus, the IBR is able to generate $|I_P^+|$ in Step 3 if $180° < \beta - 120° < 360°$, which is usually satisfied since β is inside [60°, 120°] as mentioned above. A similar result is obtained for other double-phase faults as well.

D. Compensation of Shunt Capacitor's Current

One of the differences between the method developed in Section IV and previous studies (such as [6]–[8], [10], [12], [13]) is that this method factors in the current of the LC filter's shunt capacitor ($I_{Q\text{-cap}}$) in the formulation that derives the reference current. This would marginally impact the reference currents derived in Section IV. The following explains the rationale behind the approach adopted in this paper. $I_{Q\text{-cap}}$ is an uncontrolled current that is added to the currents of the inverter switches before the POC. Thus, if $I_{Q\text{-cap}}$ is neglected when the reference currents are calculated, the superimposed reactive currents measured at the POC will deviate slightly from what the GC requires. This error was compensated for the positive-sequence circuit in (4a) by subtracting $|I_{Q\text{-cap}}^+|$ from the required reactive current at the POC, i.e., $|\pm|I_{Q\text{-pre}}^+| + \Delta I_Q^+|$. Similarly, $\Delta I_{Q\text{-cap}}^-$ was added to the required negative-sequence reactive current at

TABLE I
TOTAL ACTIVE AND REACTIVE POWERS OF THE 16 IBRS IN THE IEEE 39-BUS TEST SYSTEM

Case No.	Fault location	Fault type	K-factor	Method of [8] and [9]			Proposed method (without capacitor's current compensation)			Proposed method (with capacitor's current compensation)		
				P^+ (MW)	Q^+ (MVAr)	Q^- (MVAr)	P^+ (MW)	Q^+ (MVAr)	Q^- (MVAr)	P^+ (MW)	Q^+ (MVAr)	Q^- (MVAr)
1	B3	AG	2	2437	870	99	2471	884	103	2476	800	103
2	B3	AG	4	1712	1389	112	1781	1445	118	1813	1372	118
3	B3	AG	6	833	1762	105	1051	1920	112	1093	1862	112
4	B3	BC	2	2121	885	169	2219	882	169	2222	810	170
5	B3	BC	4	1096	1452	200	1472	1456	201	1492	1398	202
6	B3	BC	6	357	1697	196	800	1734	199	823	1693	200
7	B3	BCG	2	2076	1097	64	2098	1096	64	2117	1028	64
8	B3	BCG	4	1177	1862	80	1424	1860	81	1467	1805	81
9	B3	BCG	6	388	2155	81	706	2179	81	738	2146	82
10	B16	AG	2	1836	1065	190	1880	1092	198	1895	1017	199
11	B16	AG	4	816	1522	209	908	1684	226	934	1628	227
12	B16	AG	6	475	1685	206	535	1944	222	556	1902	224
13	B16	BC	2	1500	1005	296	1663	1005	297	1669	944	300
14	B16	BC	4	586	1395	326	892	1414	327	907	1370	331
15	B16	BC	6	288	1503	325	606	1535	325	609	1500	329
16	B16	BCG	2	1483	1227	95	1527	1226	95	1547	1174	97
17	B16	BCG	4	604	1754	110	767	1763	110	789	1728	112
18	B16	BCG	6	300	1889	111	484	1902	111	492	1877	113

the POC (i.e., ΔI_Q^-) in (4b) to derive $|I_Q^-|$. Thus, when $I_{Q\text{-cap}}^{\pm}$ is taken into account, the IBR generates smaller positive- and larger negative-sequence reactive currents, compared to when $I_{Q\text{-cap}}^{\pm}$ is neglected.

Since the positive-sequence voltage at the POC never drops below the negative-sequence voltage, $|I_{Q\text{-cap}}^{+}|$ always exceeds $|I_{Q\text{-cap}}^{-}|$. Therefore, when $I_{Q\text{-cap}}^{\pm}$ is taken into account, the decrease in the positive-sequence reactive current is larger than the increase in the negative-sequence reactive current. Therefore, besides the absolute precision in complying with the GC, considering $I_{Q\text{-cap}}^{\pm}$ in the formulation creates more room to generate active current.

VI. PERFORMANCE EVALUATION

This section investigates the benefits of the proposed solution from a system-side perspective when the penetration level of IBRs is high. Subsequently, the performance of this method and the state-of-the-art literature on GC compliance will be compared.

A. System-Wide Impacts

Maximum utilization of the IBRs' current generation capacity achieved by the proposed method enhances the grid stability from the following perspectives:

- The GCs mandate that after the LVRT, the IBRs ramp up the active power to the pre-LVRT level quickly to prevent instability [18]. However, high ramp rates for the active power can cause voltage fluctuations if the grid is not strong [16]—a common scenario with the increased penetration of IBRs. Maximizing the IBRs' active power during the LVRT enables the IBR to return to the pre-LVRT level of active power without the need for a high ramp rate and improves frequency stability of the grid after the LVRT conditions [18].
- Maximizing the IBRs' reactive current elaborated in Section V-A improves the grid's short-term voltage stability and fault-induced delayed voltage recovery [19].

This section presents a comparative analysis to show the system-wide impact made by the proposed method in increasing the power of the IBRs across the grid shown in Fig. 2. Table I shows the total active and reactive power (P and Q) generated by the IBRs in Fig. 2 using three methods for different fault locations, fault types, and IBR K-factors. Columns 5 to 7 report the results for the method used in the available literature, such as [8] and [9], which involves (1) explained in Section III. Since this method does not consider $I_{Q\text{-cap}}^{\pm}$ in the formulation of reference currents (Section V-D), it cannot be directly compared with the algorithm developed in Section IV. For a better comparison, therefore, Table I reports the results for two versions of the proposed method: the version reported in columns 11 to 13 strictly follows the relations in Section IV; the other version in columns 8 to 10 removes $I_{Q\text{-cap}}^{\pm}$ from (4) to neglect the capacitor's effect, enabling direct comparison with [8] and [9].

1) Positive-Sequence Powers: Columns 5 and 8 of Table I indicate the for all fault conditions P^+ of the proposed method is larger. Consider, for example, Case 6 with $K = 6$ in Table I. The total active power generated by the IBRs using the proposed method is 443 MW (124%) larger than the total active power when the methods of [8] and [9] are used. A noticeable pattern for P^+ in Table I is that as the K-factor increases, the active power generated by the proposed method becomes more superior. For instance, for a BC fault at bus B16, and for $K = 2$, $K = 4$, and $K = 6$, the proposed method generates 163 MW (11%), 306 MW (52%), and 318 MW (110%), respectively, more than existing methods. The reason is that for larger K-factors, existing methods do not attempt to generate any active current after scaling down the reactive currents. For the proposed method,

however, large amounts of active current can be generated in Step 3.

As discussed in Section V-A, the superiority of the proposed method lies in the generation of not only larger active power, but also higher levels of reactive power. As shown in Table I, the improvement in the reactive power is more significant for cases involving single-line-to-ground faults and large K-factors. These are the cases for which the reactive currents need to be scaled down due to the large K-factor even though the voltage drop at the POC is not very severe. In Case 12 in Table I, for example, the IBRs generate 259 MVAr (15%) of extra reactive if they use the proposed method. For the same case, the proposed method generates 64 MW (13%) of additional active power as well. Only in three cases with lower K-factor, the Q^+ generated by the proposed method is 1 to 3 MVAr smaller. For instance, the Q^+ given by the proposed method is 882 MVAr, while the method in [8] and [9] yields 885 MVAr; i.e., a mere 0.34% difference. This stems from the fact that for the method in [8] and [9], the dip in the positive-sequence voltage during the transients of the first cycle of the fault is larger. The first cycle of the fault is when the K-factor diagram in Fig. 1 is used to calculate ΔI_Q^+. Therefore, a larger reactive current is obtained by the K-factor diagram.

2) Negative-Sequence Reactive Power: Comparison of columns 7 and 10 reveals that the proposed method generates larger Q^- for all of the cases. Meanwhile, the pattern of variations for Q^- is different from what is observed for Q^+. As the K-factor increases, Q^+ generated by IBRs naturally increases for all of the three methods in Table I. Similarly, Q^- increases in columns 7, 10, and 13 as K is increased from 2 to 4. However, in most cases, from $K = 4$ to $K = 6$, Q^- decreases. The reason is that from $K = 4$ to $K = 6$, the generation of larger amount of Q^+ causes the system to become more balanced, with larger positive-sequence voltage and smaller negative-sequence voltage throughout the grid.

3) Effect of Compensating Shunt Capacitor's Current: As explained in Section V-D, compensating for the capacitor's currents enables the IBR to generate larger active currents. This issue can be observed by comparing P^+ in columns 8 and 11 of Table I. Furthermore, a comparison between the reactive currents of these two methods confirms the discussion in Section V-D that when an IBR compensates for the current of the shunt capacitor, Q^+ decreases and Q^- increases. The numbers for Q^- seem to stay unchanged in some cases. This is due to the rounding error. For instance, Q^- in Case 1 in Table I for the proposed method without and with compensation of the capacitor's current is 103.00 MVAr and 103.13 MVAr, respectively.

B. Comparative Analysis

To the best of the authors' knowledge, the state-of-the-art methods for compliance with recent GCs have been published in [8], [6], and [11]. In [8], the phase current magnitudes are formulated as the scalar sum of $|I^+|$ and $|I^-|$, as opposed to the actual vector sum relation between the phase and sequence currents. Section IV-A demonstrated that the inverter power obtained by the proposed method is larger than the power obtained by the different formulation of [8]. In [6], the relation considered in (19) of that paper between the phase and sequence currents holds only when the angle between I^+ and I^- is 45°, which is not valid during most LVRT conditions. Among the aforementioned three papers, the full range of possible angles between I^+ and I^- is considered only in [11]. Therefore, this section presents a detailed comparative analysis between the proposed method and the technique developed in [11].

The method proposed in Section IV of [11] has six steps, which focus on deriving the setpoints for the inverter's power, not current. This process is different from following the explicit superimposed reactive currents given by the GCs in Fig. 1—i.e., the approach adopted in this paper—and results in IBR currents that are not compliant with recent GCs and standards for the following main reasons.

1) The method in [11] relies on the calculation of the inverter's maximum total reactive power, $Q_{\max}$. For a given LVRT condition, $Q_{\max}$ is calculated in [11] by setting the active power reference to zero and finding the reactive power that makes the maximum phase current equal to the IBR's current limit. However, Section V-B, including Case 4, demonstrated that depending on the angles/magnitudes of the sequence currents, the maximum reactive current of an IBR can potentially be obtained when the active current is not zero. This renders the formulation for $Q_{\max}$ in [11] invalid.
2) An inverter's LVRT currents must satisfy (21) obtained from Fig. 1 (which is also expressed as (27) in [11]).

$$\Delta I_Q^{\pm} = k^{\pm} \Delta V^{\pm} \tag{21}$$

In this relation, $k^{\pm}$ denotes the K-factors for the positive and negative sequences. However, if the inverter's operating point satisfies the condition for the second row of (30) and (31) of [11], those equations return $Q^+ = k^+ Q_{\max}(1 - V^+)$ and $Q^- = k^- Q_{\max} V^-$. Dividing these sequence reactive powers over their respective sequence voltages yields

$$|I_Q^+| = \frac{k^+ Q_{\max}(1 - V^+)}{V^+} \tag{22a}$$

$$|I_Q^-| = k^- Q_{\max} \tag{22b}$$

The reactive current given by (22) is different from the current required by the GCs and expressed by (21). The comparison between (21) and (22) becomes easier if the pre-fault reactive currents are assumed to be zero, making $\Delta I_Q^{\pm}$ equal to $|I_Q^{\pm}|$. It can be shown that a similar discrepancy exists between the currents given by [11] and (21) if the inverter's operating point satisfies the condition in the third rows of (30) and (31) in [11].
3) The additional negative-sequence reactive current required by the IEEE 2800 standard during LVRT shall not exceed the additional positive-sequence reactive current [16]. In addition, the positive-sequence current obtained from the curve in Fig. 1 is equal to or larger than the negative-sequence current for the typical pairs of ΔV^+ and ΔV^- of actual power system faults. The

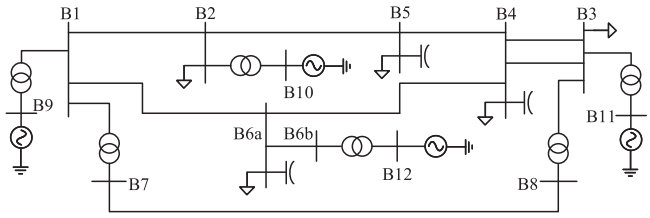

Fig. 16. The CIGRE North American high-voltage benchmark system [20].

relative magnitude of sequence currents given by [11] can be determined using (30) of [11] and (22) derived above. The condition for the second row in (30) of [11] is $1-1/k^+ < V^+ < 0.9$, which can be written as $0.11 < \frac{1-V^+}{V^+} < \frac{1}{k^+-1}$. The upper boundary of this inequality is less than 1 because $2 \le k^+ \le 6$. Therefore, $\frac{1-V^+}{V^+}$ in (22a) is below 1. Thus, if $k^+ = k^-$ (which is always the case in [3]), $|I_Q^+|$ given by (22a) becomes smaller than $|I_Q^-|$ given by (22b). This problem can also occur when the inverter's operating point satisfies the condition for the third row of (30) in [11]. If k_2 given by (33) of [11] is below 0.5, then $Q^- > Q^+$ in (29) of [11]. Since V^+ is always greater than V^-, this will lead to $|I_Q^+| < |I_Q^-|$. Even when $k_2 > 0.5$, since $V^+ > V^-$, although $Q^+ > Q^-$, $|I_Q^-|$ may be larger than $|I_Q^+|$. Thus, $|I_Q^-|$ given by [11] is larger than $|I_Q^+|$ in most fault conditions. This can be observed in Figs. 6, 8, 9, 11, 12, and 14 of [11]. Inefficient utilization of the inverter's capacity and generation of more $|I_Q^-|$ than $|I_Q^+|$ can jeopardize the IBRs' dynamic voltage support, which is the main purpose of the GCs' requirement for reactive current generation during LVRT.

Considering the above issues, the following case study compares the proposed method with the method of [11].

Case 5: The mathematical formulations in the paper do not rely on any information about the grid topology and the number of IBRs in the grid. To further demonstrate the independence of the proposed method from the grid conditions, this case study uses a different test system. Fig. 16 shows the CIGRE North American high-voltage network—whose specifications are given in [20]. In the system of Fig. 16, the synchronous generator connected to bus B11 and its step-up transformer are replaced with a 34.5-kV, 100-MW IBR plant, which is interfaced to the grid through a 150-MVA, 230-kV/34.5-kV, YGd1 transformer. The HV side of this transformer is connected to bus B3 via a 50-km tie-line. The phase current limit of the IBR is $I_{\max} = 1.2$ pu. Prior to the fault, the IBR is working at unity power factor at the POM, corresponding to $|I_{Q\text{-pre}}| = 0.05$ pu at the POC. At $t = 1$ s, an AG fault occurs in the middle of one of the parallel lines that connect buses B3 and B4. In the following analysis, the steady-state fault voltage is used to determine the current reference because the power-based formulation in [11] requires continuous measurement of voltage.

Fig. 17 displays the results obtained for the above LVRT condition when $K = 2$ and the IBR uses the method of [11] (considering that the negative sign for the second term on the

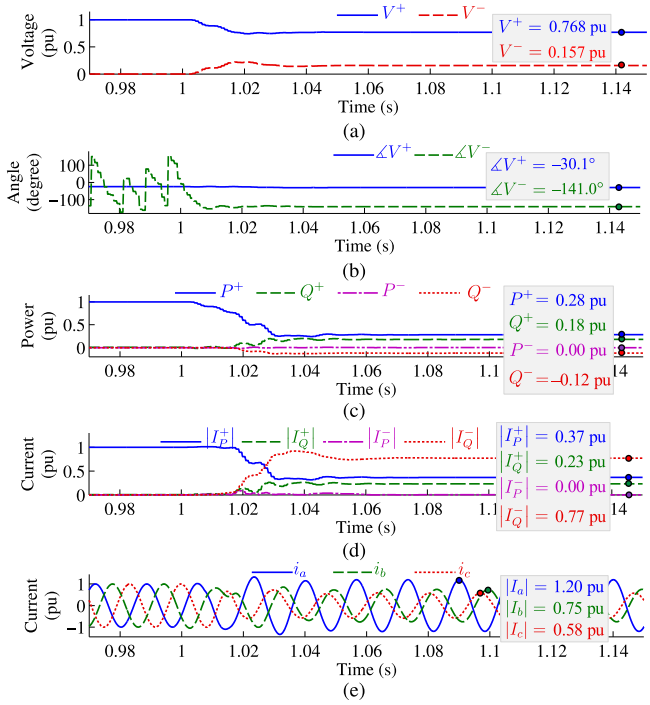

Fig. 17. Measurements for Case 5 and $K = 2$ using [11], (a) Sequence voltage magnitudes, (b) Sequence voltage angles, (c) Sequence powers, (d) Active and reactive sequence currents, (e) Instantaneous currents.

right side of (34) of [11] is a typographical error and must be positive). The voltages in Fig. 17(a) and (b) correspond to $\Delta V^+ = 0.232$ pu and $\Delta V^- = 0.157$ pu, for which the curve in Fig. 1 returns $|\Delta I_Q^+| = 0.464$ pu and $|\Delta I_Q^-| = 0.314$ pu. The method in [11] regulates the sequence powers and yields the curves shown in Fig. 17(c). Dividing these sequence power over their respective sequence voltages results in $|I_Q^+| = 0.23$ pu and $|I_Q^-| = 0.77$ pu (measured before the LC filter's capacitor). Since the pre-fault reactive current is $|I_{Q\text{-pre}}| = 0.047$ pu and the shunt capacitor's current is $|I_{Q\text{-cap}}^+| = 0.032$ pu and $|I_{Q\text{-cap}}^-| = 0.008$ pu, the superimposed currents generated by the IBR are $|\Delta I_Q^+| = 0.22$ pu and $|\Delta I_Q^-| = 0.76$ pu (from (4)). This confirms the above analysis that the superimposed reactive currents obtained by the method of [11] are different from the currents required by the GCs (in this case, $|\Delta I_Q^+| = 0.464$ pu and $|\Delta I_Q^-| = 0.314$ pu).

This discrepancy is particularly problematic due to the very large negative-sequence current, which is more than triple the positive-sequence reactive current. This large negative-sequence current prevents the inverter from generating a larger positive-sequence reactive current for dynamic voltage support. In addition, as shown by the instantaneous currents of Fig. 17(e), although the method of [11] has maximized current of phase A, the excessive negative-sequence current changes the rotation of three phase currents from ABC to ACB during the fault.

Increasing the inverter's K-factor exacerbates this problem. The measurements for the same fault condition are shown in Fig. 18. The sequence voltage and power curves of Fig. 18(a)–(c) yield the sequence current curves of Fig. 18(d), in which I_Q^- consumes almost 1 pu of the inverter's current generation

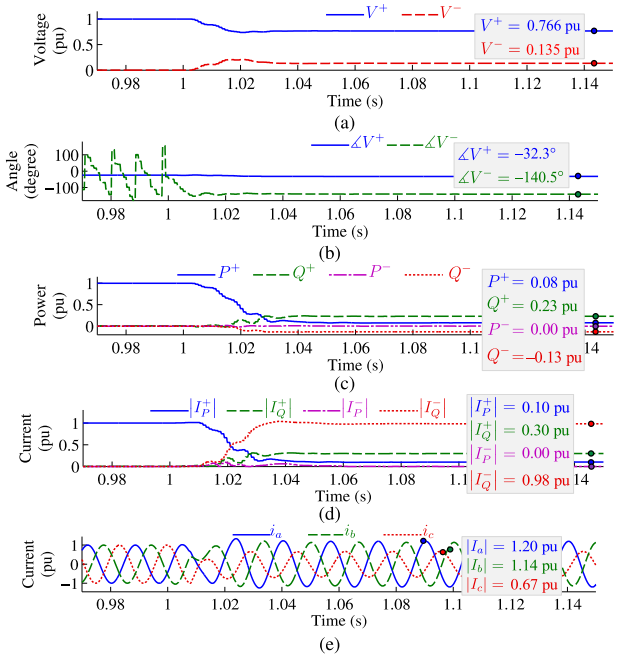

Fig. 18. Measurements for Case 5 and $K = 4$ using [11], (a) Sequence voltage magnitudes, (b) Sequence voltage angles, (c) Sequence powers, (d) Active and reactive sequence currents, (e) Instantaneous currents.

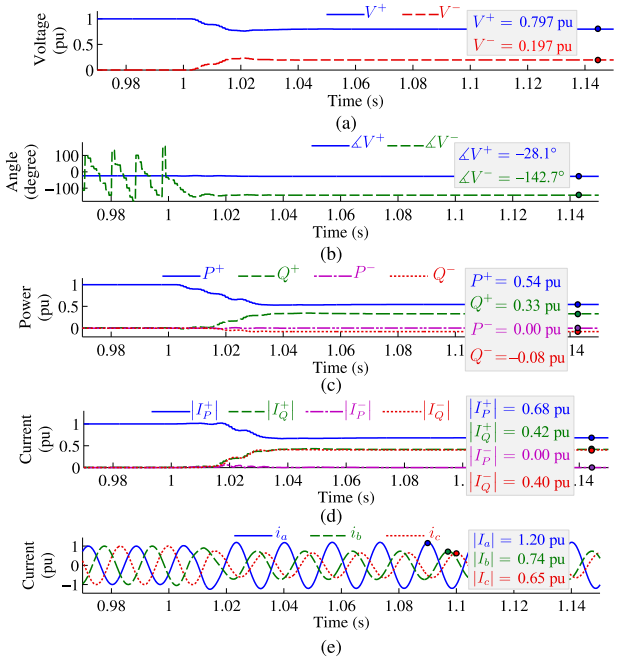

Fig. 19. Measurements for Case 5 and $K = 2$ using the proposed method, (a) Sequence voltage magnitudes, (b) Sequence voltage angles, (c) Sequence powers, (d) Active and reactive sequence currents, (e) Instantaneous currents.

capacity, hence a lower dynamic support for the voltage and an obvious ACB rotation for phase currents in Fig. 18(e).

The performance of the proposed method for the same LVRT conditions is shown in Fig. 19 for K =2. In Fig. 19(a), $\Delta V^+ = 0.203$ pu and $\Delta V^- = 0.197$ pu. For these voltage changes, the curve in Fig. 1 returns $|\Delta I_Q^+| = 0.406$ pu and $|\Delta I_Q^-| = 0.394$ pu. Plugging these two currents along with the pre-fault and

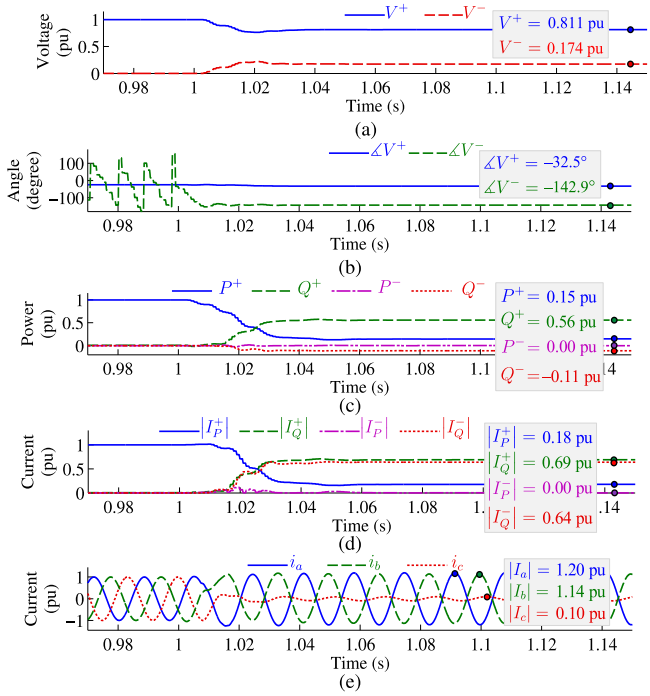

Fig. 20. Measurements for Case 5 and $K = 4$ using the proposed method, (a) Sequence voltage magnitudes, (b) Sequence voltage angles, (c) Sequence powers, (d) Active and reactive sequence currents, (e) Instantaneous currents.

the capacitor's reactive currents in (4) yields the reactive current setpoints of $|I_Q^+| = 0.42$ pu and $|I_Q^-| = 0.40$ pu. The reactive currents in Fig. 19(d) are identical with these GC-compliant reactive currents. Besides compliance with the GCs, the phase currents maintain their ABC rotation in Fig. 19(e). More importantly, the positive-sequence voltage obtained by the proposed method in Fig. 19(a) is 3% higher than the respective voltage obtained by the method of [11] in Fig. 17(a). The difference between the voltages obtained by the two methods naturally increases if the number and/or rating of IBRs increase beyond the single 100-MW unit that has been considered in Fig. 16. The results obtained by the proposed method for K =4 are shown in Fig. 20, demonstrating strict compliance with the curve of Fig. 1. This makes V^+ of [11] in Fig. 20(a) 4% higher than V^+ in Fig. 18(a).

Further simulation results are presented in Tables II–IV to compare the proposed method and [11]. Table II shows the total active and reactive powers and the positive-sequence voltage for different fault types and K-factors when the IBR of Case 5 implements the method of [11] and the proposed method. For all fault types and K-factors, Q^- generated by [11] is larger than that obtained by the proposed method, resulting in the same problems that were discussed for Case 5. An interesting observation is that the difference between Q^+ of these two methods in each row of Table II is larger than the difference between their Q^-'s. This is due to the fact that V^- is always smaller than V^+, so Q^- given by [11] is only slightly larger even though [11] utilizes a substantial capacity of the IBR to generate $|I_Q^-|$. On the other hand, by generating GC-compliant I_Q^- and utilizing the rest of the IBR's capacity for the positive-sequence

TABLE II
ACTIVE AND REACTIVE POWERS AND THE POSITIVE-SEQUENCE VOLTAGE OF THE IBR CONNECTED TO B3 IN FIG. 16 FOR THE FAULT LOCATION OF CASE 5

Fault type	K-factor	P^+ (MW)		Q^+ (MVAr)		Q^- (MVAr)		V^+ (pu)	
		Method of [11]	Proposed Method	Method of [11]	Proposed Method	Method of [11]	Proposed Method	Method of [11]	Proposed Method
AG	2	28	54	18	33	12	8	0.77	0.80
AG	4	8	15	23	56	13	11	0.77	0.81
AG	6	8	15	23	56	13	11	0.77	0.81
BC	2	7	5	29	38	25	21	0.60	0.62
BC	4	7	5	29	38	25	21	0.60	0.62
BC	6	7	5	29	38	25	21	0.60	0.62
BCG	2	8	6	30	40	17	13	0.52	0.53
BCG	4	8	6	30	40	17	13	0.52	0.53
BCG	6	8	6	30	40	17	13	0.52	0.53

TABLE III
ACTIVE AND REACTIVE POWERS AND THE POSITIVE-SEQUENCE VOLTAGE MAGNITUDE OF THE IBR CONNECTED TO B6B IN FIG. 16 FOR FAULTS ON B6A

Fault type	K-factor	P^+ (MW)		Q^+ (MVAr)		Q^- (MVAr)		V^+ (pu)	
		Method of [11]	Proposed Method	Method of [11]	Proposed Method	Method of [11]	Proposed Method	Method of [11]	Proposed Method
AG	2	14	58	60	82	34	28	0.66	0.71
AG	4	14	18	60	102	34	32	0.66	0.71
AG	6	14	18	60	102	34	32	0.66	0.71
BC	2	0	0	60	66	52	48	0.52	0.53
BC	4	0	0	60	66	52	48	0.52	0.53
BC	6	0	0	60	66	52	48	0.52	0.53
BCG	2	0	0	56	64	17	22	0.38	0.39
BCG	4	0	0	56	64	17	22	0.38	0.39
BCG	6	0	0	56	64	17	22	0.38	0.39

TABLE IV
ACTIVE AND REACTIVE POWERS AND THE POSITIVE-SEQUENCE VOLTAGE MAGNITUDE OF THE IBR CONNECTED TO B6B IN FIG. 16 FOR FAULTS ON B1

Fault type	K-factor	P^+ (MW)		Q^+ (MVAr)		Q^- (MVAr)		V^+ (pu)	
		Method of [11]	Proposed Method	Method of [11]	Proposed Method	Method of [11]	Proposed Method	Method of [11]	Proposed Method
AG	2	No LVRT	No LVRT	No LVRT	No LVRT	No LVRT	No LVRT	No LVRT	No LVRT
AG	4	No LVRT	No LVRT	No LVRT	No LVRT	No LVRT	No LVRT	No LVRT	No LVRT
AG	6	No LVRT	No LVRT	No LVRT	No LVRT	No LVRT	No LVRT	No LVRT	No LVRT
BC	2	0	78	54	78	30	26	0.67	0.72
BC	4	0	0	54	92	30	28	0.67	0.72
BC	6	0	0	54	92	30	28	0.67	0.72
BCG	2	0	78	54	78	30	26	0.67	0.72
BCG	4	0	0	54	92	30	28	0.67	0.72
BCG	6	0	0	54	92	30	28	0.67	0.72

current, the proposed method offers a significantly larger Q^+. This can be observed by comparing columns 5 to 8 in Table II. The above differences between [11] and the proposed method are ultimately reflected in the positive-sequence voltage reported in the last two columns of the table. In all cases, the proposed method exhibits superior dynamic voltage support. Both methods are able to maximize their active powers (for their own positive- and negative- sequence reactive powers). The difference in the active powers of the two methods stems from the difference in their reactive powers.

In order to test another topology and IBR rating, the synchronous generator connected to B12 in Fig. 16 and its step-up transformer are replaced with a 34.5-kV, 200-MW IBR plant which is interfaced to the grid through a 250-MVA, 230-kV/34.5-kV, YGd1 transformer. Tables III and IV show the results for different faults on buses B6a and B1, respectively. Both of these tables confirm the previous findings. Note that for AG faults at B1, ΔV^+ and ΔV^- are both in the 0.1-pu dead-band of Fig. 1, and neither method enters the LVRT mode.

VII. CONCLUSION

This paper demonstrated that existing literature on inverter control does not satisfy the requirements of recent GCs for maximum active and reactive current generation during LVRT. The available techniques that use the scalar sum of the sequence currents to derive the inverter reference currents lead to miscalculation of an IBR's capacity for generating active current. This may also cause unnecessary reduction of the reactive currents without any active current generation. The solution

developed in the paper addressed all of these problems and maximized both the active and reactive currents of an IBR. In particular, the paper showed that when the reactive currents make the phase currents exceed the IBR's limit, it is possible to generate non-negligible amounts of active current and bring the phase currents below their limit without scaling down the reactive currents. Additionally, the proposed method derived a larger scaling factor and so maximized the reactive current generated by the IBR. It was also shown that after scaling down the reactive currents, although at least one of the phase currents reaches the IBR's limit, the IBR is still usually capable of generating active current. Furthermore, a detailed comparative study verified the superiority of the proposed method over the state-of-the-art literature with respect to GC compliance and dynamic voltage support during the LVRT.

REFERENCES

[1] *Grid Connection Regulations for High and Extra High Voltage*, E.ON Netz GmbH, Bayreuth, Apr. 2006. [Online]. Available: https://bit.ly/36q8mJt

[2] *The Grid Code*, National Grid Electricity System Operator Limited, Mar. 2017. [Online]. Available: https://bit.ly/35ktXE4

[3] *Technical Requirements for the Connection and Operation of Customer Installations to the Extra High Voltage Network (TAR Extra High Voltage)*, VDE-AR-N 4130, Berlin, Nov. 2018. [Online]. Available: https://bit.ly/2SKOoD6

[4] *Requirements for Generating Plants to be Connected in Parallel with Distribution Networks - Part 2: Connection to an MV Distribution Network - Generating Plants Up to and Including Type B, CLC/TC 8X*, Brussels, Jan. 2019. [Online]. Available: https://bit.ly/3lE3tTb

[5] N. Bottrell and T. C. Green, "Comparison of current-limiting strategies during fault ride-through of inverters to prevent latch-up and wind-up," *IEEE Trans. Power Electron.*, vol. 29, no. 7, pp. 3786–3797, Jul. 2014.

[6] P. Sochor, N. M. L. Tan, and H. Akagi, "Low-voltage-ride-through control of a modular multilevel single-delta bridge-cell (SDBC) inverter for utility-scale photovoltaic systems," *IEEE Trans. Ind Appl.*, vol. 54, no. 5, pp. 4739–4751, Sep./Oct. 2018.

[7] M. A. Garnica López, J. L. García de Vicuña, J. Miret, M. Castilla, and R. Guzmán, "Control strategy for grid-connected three-phase inverters during voltage sags to meet grid codes and to maximize power delivery capability," *IEEE Trans. Power Electron.*, vol. 33, no. 11, pp. 9360–9374, Nov. 2018.

[8] X. Liu et al., "Fault current hierarchical limitation strategy for fault ride-through scheme of microgrid," *IEEE Trans. Smart Grid*, vol. 10, no. 6, pp. 6566–6579, Nov. 2019.

[9] M. A. Azzouz, A. Hooshyar, and E. F. El-Saadany, "Resilience enhancement of microgrids with inverter-interfaced DGs by enabling faulty phase selection," *IEEE Trans. Smart Grid*, vol. 9, no. 6, pp. 6578–6589, Nov. 2018.

[10] D. Shin, K.-J. Lee, J.-P. Lee, D.-W. Yoo, and H.-J. Kim, "Implementation of fault ride-through techniques of grid-connected inverter for distributed energy resources with adaptive low-pass notch PLL," *IEEE Trans. Power Electron.*, vol. 30, no. 5, pp. 2859–2871, May 2015.

[11] M. G. Taul, X. Wang, P. Davari, and F. Blaabjerg, "Current reference generation based on next-generation grid code requirements of grid-tied converters during asymmetrical faults," *IEEE Trans. Emerg. Sel. Topics Power Electron.*, vol. 8, no. 4, pp. 3784–3797, Dec. 2020.

[12] D. I. Brandao, F. E. G. Mendes, R. V. Ferreira, S. M. Silva, and I. A. Pires, "Active and reactive power injection strategies for three-phase four-wire inverters during symmetrical/asymmetrical voltage sags," *IEEE Trans. Ind Appl.*, vol. 55, no. 3, pp. 2347–2355, May/Jun. 2019.

[13] M. Islam, M. Nadarajah, and M. J. Hossain, "A grid-support strategy with PV units to boost short-term voltage stability under asymmetrical faults," *IEEE Trans. Power Syst.*, vol. 35, no. 2, pp. 1120–1131, Mar. 2020.

[14] A. Camacho, M. Castilla, J. Miret, A. Borrell, and L. G. de Vicuña, "Active and reactive power strategies with peak current limitation for distributed generation inverters during unbalanced grid faults," *IEEE Trans. Ind. Electron.*, vol. 62, no. 3, pp. 1515–1525, Mar. 2015.

[15] IEEE 39-bus system, 2013. [Online]. Available: https://bit.ly/33VuknB

[16] *IEEE Draft Standard for Interconnection and Interoperability of Inverter-Based Resources (IBR) Interconnecting with Associated Transmission Electric Power Systems*, IEEE Standard 2800, Oct. 2021.

[17] A. Hooshyar, E. F. El-Saadany, and M. Sanaye-Pasand, "Fault type classification in microgrids including photovoltaic DGs," *IEEE Trans. Smart Grid*, vol. 7, no. 5, pp. 2218–2229, Sep. 2016.

[18] B. Weise, "Impact of K-factor and active current reduction during fault-ride-through of generating units connected via voltage-sourced converters on power system stability," *IET Renewable Power Gener.*, vol. 9, pp. 25–36, Jan. 2015.

[19] G. Lammert, D. Premm, L. D. P. Ospina, J. C. Boemer, M. Braun, and T. Van Cutsem, "Control of photovoltaic systems for enhanced short-term voltage stability and recovery," *IEEE Trans. Energy Convers.*, vol. 34, no. 1, pp. 243–254, Mar. 2019.

[20] "Benchmark systems for network integration of renewable and distributed energy resources," CIGRE, Paris, France, Tech. Rep. C6.04.02, Apr. 2014.

Ali Azizi received the B.Sc. and M.Sc. degrees in electrical engineering from the University of Tehran, Tehran, Iran, in 2017 and 2019, respectively. He is currently working toward the Ph.D. degree with the Center for Applied Power Electronics, University of Toronto, Toronto, ON, Canada. His research interests include control and protection of inverter-based resources. Mr. Azizi has been recognized as one of the exceptional reviewers of IEEE TRANSACTIONS ON POWER DELIVERY in 2020 and 2021

Amin Banaiemoqadam received the Ph.D. degree in electrical and computer engineering from the University of Toronto, Toronto, ON, Canada, in 2021. He is currently working as a Lead Engineer with GE Renewable Energy, Markham, ON, Canada. He is a Member of several IEEE standards and different working groups of IEEE Power System Relaying and Control (PSRC) committee. He has also been recognized as one of the exceptional reviewers of IEEE TRANSACTIONS ON POWER DELIVERY in 2019 and 2020. His work focuses on protection and control of inverter-based resources.

Ali Hooshyar (Senior Member, IEEE) is currently a Canada Research Chair in Electric Power Systems with the Electrical and Computer Engineering Department of the University of Toronto, Toronto, ON, Canada. His research interests include protection and control of renewable energy systems, and smart grids. Dr. Hooshyar is the Editor of the IEEE TRANSACTIONS ON SMART GRID, IEEE TRANSACTION ON POWER DELIVERY, and IEEE POWER ENGINEERING LETTERS. He is the Guest Editor-in-Chief of the Special Issue of the IEEE TRANSACTIONS ON POWER DELIVERY on Resilience-Oriented Protection, Control, and Monitoring Systems for Power Grids. He is also an Associate Editor for the Wiley Encyclopedia of Electrical and Electronics Engineering.

Manish Patel (Senior Member, IEEE) received the B.E. degree in electrical engineering from B.V.M. Engineering College, V.V. Nagar, India in 2000 and the Ph.D. degree in electrical engineering from Clemson University, Clemson, SC, USA, in 2009. He joined Georgia Power Company in 2006 as a Protection & Control Applications Engineer. Since then, he has spent eight years in Protection & Control Applications and six years with Transmission Planning – Stability group. He is currently a Chief Engineer with the Protection & Control Applications Department. He is an Active Member of the IEEE PSRCC. He is also a Vice Chair and Secretary of the IEEE P2800 and IEEE P2800.2 Working Groups respectively. He is a registered Professional Engineer with the State of Alabama.